

1 **A population-level invasion by transposable**
2 **elements triggers genome expansion in a fungal**
3 **pathogen**

4
5
6 Ursula Oggenfuss¹, Thomas Badet¹, Thomas Wicker², Fanny E. Hartmann^{3,4}, Nikhil K. Singh¹, Leen
7 N. Abraham¹, Petteri Karisto^{4,6}, Tiziana Vonlanthen⁴, Christopher C. Mundt⁵, Bruce A. McDonald⁴,
8 Daniel Croll^{1,*}

9
10
11 ¹ Laboratory of Evolutionary Genetics, Institute of Biology, University of Neuchâtel, 2000 Neuchâtel,
12 Switzerland

13 ² Institute for Plant and Microbial Biology, University of Zurich, Zurich, Switzerland

14 ³ Ecologie Systématique Evolution, Bâtiment 360, Univ. Paris-Sud, AgroParisTech, CNRS,
15 Université Paris-Saclay, 91400 Orsay, France

16 ⁴ Plant Pathology, Institute of Integrative Biology, ETH Zurich, Zurich, Switzerland

17 ⁵ Department of Botany and Plant Pathology, Oregon State University, Corvallis, OR 97331-2902,
18 USA

19 ⁶ Department of Evolutionary Biology and Environmental Studies, University of Zurich, Zurich,
20 Switzerland

21
22 * Author for correspondence: daniel.croll@unine.ch

23

24

25

26

27

28

29

30 Running title: Transposable element invasion triggers genome expansion

31 **ABSTRACT**

32 Genome evolution is driven by the activity of transposable elements (TEs). The spread of TEs can
33 have deleterious effects including the destabilization of genome integrity and expansions. However,
34 the precise triggers of genome expansions remain poorly understood because genome size evolution
35 is typically investigated only among deeply divergent lineages. Here, we use a large population
36 genomics dataset of 284 individuals from populations across the globe of *Zymoseptoria tritici*, a
37 major fungal wheat pathogen. We built a robust map of genome-wide TE insertions and deletions to
38 track a total of 2,456 polymorphic loci within the species. We show that purifying selection
39 substantially depressed TE frequencies in most populations but some rare TEs have recently risen in
40 frequency and likely confer benefits. We found that specific TE families have undergone a
41 substantial genome-wide expansion from the pathogen's center of origin to more recently founded
42 populations. The most dramatic increase in TE insertions occurred between a pair of North
43 American populations collected in the same field at an interval of 25 years. We find that both
44 genome-wide counts of TE insertions and genome size have increased with colonization bottlenecks.
45 Hence, the demographic history likely played a major role in shaping genome evolution within the
46 species. We show that both the activation of specific TEs and relaxed purifying selection underpin
47 this incipient expansion of the genome. Our study establishes a model to recapitulate TE-driven
48 genome evolution over deeper evolutionary timescales.

49

50 INTRODUCTION

51 Transposable elements (TEs) are mobile repetitive DNA sequences with the ability to independently
52 insert into new regions of the genome. TEs are major drivers of genome instability and epigenetic
53 change (Eichler & Sankoff, 2003). Insertion of TEs can disrupt coding sequences, trigger
54 chromosomal rearrangements, or alter expression profiles of adjacent genes (Lim, 1988; Petrov *et al.*,
55 2003; Slotkin & Martienssen, 2007; Hollister & Gaut, 2009; Oliver *et al.*, 2013). Hence, TE
56 activity can have phenotypic consequences and impact host fitness. While TE insertion dynamics are
57 driven by the selfish interest for proliferation, the impact on the host can range from beneficial to
58 highly deleterious. The most dramatic examples of TE insertions underpinned rapid adaptation of
59 populations or species (Feschotte, 2008; Chuong *et al.*, 2017), particularly following environmental
60 change or colonization events. Beneficial TE insertions are expected to experience strong positive
61 selection and rapid fixation in populations. However, most TE insertions have neutral or deleterious
62 effects upon insertions. Purifying selection is expected to rapidly eliminate deleterious insertions
63 from populations unless constrained by genetic drift (Walser *et al.*, 2006; Baucom *et al.*, 2008;
64 Cridland *et al.*, 2013; Stuart *et al.*, 2016; Lai *et al.*, 2017; Stritt *et al.*, 2017). Additionally, genomic
65 defense mechanisms can disable transposition activity. Across eukaryotes, epigenetic silencing is a
66 shared defense mechanism against TEs (Slotkin & Martienssen, 2007). Fungi evolved an additional
67 and highly specific defense system introducing repeat-induced point (RIP) mutations into any nearly
68 identical set of sequences. The relative importance of demography, selection and genomic defenses
69 determining the fate of TEs in populations remain poorly understood.

70

71 A crucial property predicting the invasion success of TEs in a genome is the transposition rate. TEs
72 tend to expand through family-specific bursts of transposition followed by prolonged phases of
73 transposition inactivity. Bursts of insertions of different retrotransposon families were observed
74 across eukaryotic lineages including *Homo sapiens*, *Zea mays*, *Oryza sativa* and *Blumeria graminis*
75 (Shen *et al.*, 1991; SanMiguel *et al.*, 1998; Eichler & Sankoff, 2003; Piegu *et al.*, 2006; Lu *et al.*,
76 2017; Frantzeskakis *et al.*, 2018). Prolonged bursts without effective counter-selection are thought to

77 underpin genome expansions. In the symbiotic fungus *Cenococcum geophilum*, the burst of TEs
78 resulted in a dramatically expanded genome compared to closely related species (Peter *et al.*, 2016).
79 Similarly, a burst of a TE family in brown hydras led to an approximately three-fold increase of the
80 genome size compared to related hydras (Wong *et al.*, 2019). Across the tree of life, genome sizes
81 vary by orders of magnitude and enlarged genomes invariably show hallmarks of historic TE
82 invasions (Kidwell, 2002). Population size variation is among the few correlates of genome size
83 across major groups, suggesting that the efficacy of selection plays an important role in controlling
84 TE activity (Lynch, 2007). Reduced selection efficacy against deleterious TE insertions is expected
85 to lead to a ratchet-like increase in genome size. In fungi, TE-rich genomes often show an isochore
86 structure alternating gene-rich and TE-rich compartments (Rouxel *et al.*, 2011). TE-rich
87 compartments often harbor rapidly evolving genes such as effector genes in pathogens or resistance
88 genes in plants (Raffaele & Kamoun, 2012; Jiao & Schneeberger, 2019). Taken together, incipient
89 genome expansions are likely driven by population-level TE insertion dynamics.

90

91 The fungal wheat pathogen *Zymoseptoria tritici* is one of the most important pathogens on crops,
92 causing high yield losses in many years (Torriani *et al.*, 2015). *Z. tritici* emerged during the
93 domestication of wheat in the Fertile Crescent where the species retained high levels of genetic
94 variation (Zhan *et al.*, 2005; Stukenbrock *et al.*, 2011). The pathogen migrated to all temperate zones
95 where wheat is currently grown and underwent multiple migration bottlenecks, in particular when
96 colonizing Oceania and North America (Zhan *et al.*, 2005; Estep *et al.*, 2015). The genome is
97 completely assembled and shows size variation between individuals sampled across the global
98 distribution range (Feurtey *et al.*, 2020; Badet *et al.*, 2020) (Goodwin *et al.*, 2011). The TE content
99 of the genome shows a striking variation of 17-24% variation among individuals (Badet *et al.*,
100 2020). *Z. tritici* recently gained major TE-mediated adaptations to colonize host plants and tolerate
101 environmental stress (Omrane *et al.*, 2015, 2017; Krishnan *et al.*, 2018; Meile *et al.*, 2018). Clusters
102 of TEs are often associated with genes encoding important pathogenicity functions (*i.e.* effectors),
103 recent gene gains or losses (Hartmann & Croll, 2017), and major chromosomal rearrangements
104 (Croll *et al.*, 2013; Plissonneau *et al.*, 2016). Transposition activity of TEs also had a genome-wide

105 impact on gene expression profiles during infection (Fouché *et al.*, 2019). The well-characterized
106 demographic history of the pathogen and evidence for recent TE-mediated adaptations make *Z.*
107 *tritici* an ideal model to recapitulate the process of TE insertion dynamics, adaptive evolution and
108 changes in genome size at the population level.

109

110 Here, we retrace the population-level context of TE insertion dynamics and genome size changes
111 across the species range by analyzing populations sampled on four continents for a total of 284
112 genomes. We developed a robust pipeline to detect newly inserted TEs using short read sequencing
113 datasets. Combining analyses of selection and knowledge of the colonization history of the
114 pathogen, we tested whether population bottlenecks were associated with substantial changes in the
115 TE content and the size of genomes.

116

117

118 **RESULTS**

119 A DYNAMIC TE LANDSCAPE SHAPED BY STRONG PURIFYING SELECTION

120 We detected 4,753 TE copies, grouped into 30 families with highly variable copy numbers in the
121 reference genome IPO323 (Figure 2 - figure supplement 1 and Figure 2 - figure supplement 2A). To
122 establish a comprehensive picture of within-species TE dynamics, we analyzed 295 genomes from a
123 worldwide set of six populations spanning the distribution range of the wheat pathogen *Z. tritici*. To
124 ascertain the presence or absence of TEs across the genome, we developed a robust pipeline (Figure
125 1A). In summary, we called TE insertions by identifying reads mapping both to a TE sequence and a
126 specific location in the reference genome. Then, we assessed the minimum sequencing coverage to
127 reliably recover TE insertions and removed 11 genomes with an average read depth below 15X
128 (Figure 1B). We tested for evidence of TEs using read depth at target site duplications (Figure 1C)
129 and scanned the genome for mapped reads indicating gaps at TE loci (Figure 1D). We found robust
130 evidence for a total of 18,864 TE insertions grouping into 2,465 individual loci. Of these loci, 35.5%
131 ($n = 876$) have singleton TEs (*i.e.*, this locus is only present in one isolate: Figure 2A, figure

132 supplement 3). An overwhelming proportion of loci (2,345 loci or 95.1%) have a TE frequency
133 below 1%. Singleton TE insertions in particular can be the product of spurious Illumina read
134 mapping errors (Nakamura *et al.*, 2011). To assess the reliability of the detected singletons, we
135 focused on seven isolates for which PacBio long-read data was available (Badet *et al.*, 2020).
136 Aligned PacBio reads confirmed the exact location of 71% (22 out of 31 singleton insertions among
137 seven isolates; see Methods for further details). We found no significant difference in read coverage
138 between confirmed and unconfirmed singleton insertions (Figure 2 - figure supplement 2C,-B and
139 Figure 2 - figure supplement 4).

140

141 The abundance of singleton TE insertions strongly supports the idea that TEs actively copy into new
142 locations but also indicates that strong purifying selection maintains nearly all TEs at low frequency
143 (Figure 2A). The density of TE loci on accessory chromosomes, which are not shared among all
144 isolates of the species, is almost twice the density found on core chromosomes (102 *versus* 58 TEs
145 per Mb; Figure 2B and Figure 2 - figure supplement 5A). This suggests relaxed selection against TE
146 insertion on the functionally dispensable and gene-poor accessory chromosomes. We found no
147 difference in TE allele frequency distribution between recombination hotspots and the rest of the
148 genome (Figure 2 - figure supplement 5B). Similarly, the TE density and the number of insertions
149 did not vary between recombination hotspots and the genomic background (Figure 2 - figure
150 supplement 5C).

151

152 TEs grouped into 23 families and 11 superfamilies, with 88.2% of all copies belonging to class
153 I/retrotransposons ($n = 2175$; Figure 2C and Figure 2 - figure supplements 6A-B). RLG/*Gypsy* ($n =$
154 1,483) and RLC/*Copia* ($n = 623$) elements constitute the largest long terminal repeats (LTR)
155 superfamilies. Class II/DNA transposons are dominated by DHH/*Helitron* ($n = 249$). As expected,
156 TE families shared among fewer isolates tend to show also lower global copy numbers (*i.e.*, all
157 isolates combined), while TE families that are present in all isolates generally have high global copy
158 numbers (Figure 2D).

159

160 We detected 153 loci with TEs inserted into genes with most of the insertions being singletons
161 (44.7%; $n = 68$) or of very low frequency (Figure 2E). Overall, TE insertions into exonic sequences
162 were less frequent than expected compared to insertions into up- and downstream regions, which is
163 consistent with effective purifying selection (Figure 2F). Insertions into introns were also strongly
164 under-represented, likely due to the small size of most fungal introns (~ 50-100 bp) and the high
165 probability of disrupting splicing or adjacent coding sequences. We also found that insertions 800-
166 1000 bp away from coding sequences of a focal gene were under-represented. Given the high gene
167 density, with an average spacing between genes of 1.744 kb, TE insertions within 800-1,000 bp of a
168 coding gene tend to be near adjacent genes already. Taken together, TEs in the species show a high
169 degree of transposition activity and are subject to strong purifying selection.

170

171 DETECTION OF CANDIDATE TE LOCI UNDERLYING RECENT ADAPTATION

172 The TE transposition activity can generate adaptive genetic variation. To identify the most likely
173 candidate loci, we analyzed insertion frequency variation among populations as an indicator for
174 recent selection. Across all populations, the insertion frequencies differed only weakly with a strong
175 skew towards extremely low F_{ST} values (mean = 0.0163; Figure 3A-B and Figure 3 - figure
176 supplement 1). To further analyze evidence for TE-mediated adaptive evolution, we screened a
177 genome-wide SNP dataset for evidence of selective sweeps using selection scans. We found 16.5 %
178 of all TE loci located in regions of selective sweep. Given our population sampling of two
179 population pairs, we tested for adaptive TE insertions in selective sweep regions either in the North
180 American or European population pairs. Hence, we selected loci having low TE insertion
181 frequencies (< 5%) in all populations except either the recent North American or European
182 population (> 20%) (Figure 3B). Based on these criteria, we obtained 7 candidate loci possibly
183 underlying local adaptation (6 in North America, one in Europe; Figure 4A and Figure 4 - figure
184 supplement 1). All loci carry inserted retrotransposons with 4 RLG_Luna, one RLG_Mercurius and
185 one RLG_Deimos.

186

187 One TE insertion is 3,815 bp downstream of a gene encoding an RTA1-like protein, which can
188 function as transporters with a transmembrane domain and have been associated with resistance
189 against several antifungal compounds (Soustre *et al.*, 1996). The insertion is also 5785 bp upstream
190 of a gene encoding a protein kinase domain (Figure 4B). The TE insertion was not detected in the
191 Middle East or the two European populations, and was at low frequencies in the Australian (3.7%)
192 and North American 1990 (1.7%) populations, but increased to 53% of all isolates in the North
193 American 2015 population (fixation index $F_{ST} = 0.42$; Figure 4 - figure supplement 1). Isolates that
194 carry the insertion show a significantly higher resistance to azole antifungal compounds (Figure 4C).
195 The TE is in the subtelomeric region of chromosome 12, with a moderate GC content, a low TE and
196 a high gene density (Figure 4D). The TE belongs to the family RLG_Luna, which shows a
197 substantial burst across different chromosomes within the species (Figures 4E-F). We found no
198 association between the phylogenetic relationships among isolates based on the two closest genes
199 and the presence or absence of the TE insertion (Figure 4G). A second candidate adaptive TE
200 insertion belongs to the RLG_Mercurius family and is located between two genes of unknown
201 function (Figure 4 - figure supplement 2). A third potentially adaptive TE insertion of a
202 RLC_Deimos is 229 bp upstream of a gene encoding a SNARE domain protein and 286 bp upstream
203 of a gene encoding a flavin amine oxidoreductase. Furthermore, the TE is inserted in a selective
204 sweep region (Figure 4 - figure supplement 2). SNARE domains play a role in vesicular transport
205 and membrane fusion (Bonifacino & Glick, 2004). An additional four candidates for adaptive TE
206 insertions belong to RLG_Luna and were located distantly to genes (Figure 4 - figure supplement 2).
207 We experimentally tested whether the TE insertions in proximity to genes were associated with
208 higher levels of fungicide resistance. For this, we measured growth rates of the fungal isolates in the
209 presence or absence of an azole fungicide widely deployed against the pathogen. We found that the
210 insertion of TEs at two loci was positively associated with higher levels of fungicide resistance,
211 suggesting that the adaptation was mediated by the TE (Figure 4C and Figure 4 - figure supplement
212 2).

213

214 POPULATION-LEVEL EXPANSIONS IN TE CONTENT

215 If TE insertion dynamics are largely neutral across populations, TE frequencies across loci should
216 reflect neutral population structure. To test this, we performed a principal component analysis based
217 on a set of six populations on four continents that represent the global genetic diversity of the
218 pathogen (Figure 5A) and 900,193 genome-wide SNPs (Figure 5B). The population structure
219 reflected the demographic history of the pathogen with clear continental differentiation and only
220 minor within-site differentiation. To account for the lower number of TE loci, we performed an
221 additional principal component analysis using a random SNP set of similar size to the number of TE
222 loci. The reduced SNP set retained the geographic signal of the broader set of SNPs (Figure 5C). In
223 stark contrast, TE frequencies across loci showed only weak clustering by geographic origin with the
224 Australian population being the most distinct (Figure 5D). We found a surprisingly strong
225 differentiation of the two North American populations sampled at a 25-year interval in the same field
226 in Oregon.

227

228 Unusual patterns in population differentiation at TE loci suggests that TE activity may substantially
229 vary across populations (Figure 6, Figure 4 - figure supplement 1). To analyze this, we first
230 identified the total TE content across all loci per isolate. We found generally lower TE numbers in
231 the Middle Eastern population from Israel (Figure 6A-C, and Figure 6 - figure supplement 1), which
232 is close to the pathogen's center of origin (Stukenbrock *et al.*, 2007). Populations that underwent at
233 least one migration bottleneck showed a substantial burst of TEs across all major superfamilies.
234 These populations included the two populations from Europe collected in 1999 and 2016 and the
235 North American population from 1990, as well as the Australian population. We found a second
236 stark increase in TE content in the North American population sampled in 2015 at the same site as
237 the population from 1990. Strikingly, the isolate with the lowest number of analyzed TEs collected
238 in 2015 was comparable to the isolate with the highest number of TEs at the same site in 1990. We
239 tested whether sequencing coverage could explain variation in the detected TEs across isolates, but
240 we found no meaningful association (Figure 2 - figure supplement 6C). We analyzed whether the
241 population-specific expansions were correlated with shifts in the frequency spectrum of TEs in the

242 populations (Figure 6D). We found that the first step of expansions observed in Europe compared to
243 the Middle East (Israel) was associated with an upwards shift in allele frequencies. This is consistent
244 with transposition activity creating new copies in the genomes and stronger purifying selection in the
245 Middle East. Similarly, the North American populations showed also signatures consistent with
246 relaxation of selection against TEs (*i.e.*, fewer low frequency TEs). We found a significant
247 difference (Two-sample Kolmogorov-Smirnov test, two-sided) in the curve shapes between the
248 population from the Middle East and North America 2015 (Figure 6 - figure supplement 2). We
249 analyzed variation in TE copy numbers across families and found that the expansions were mostly
250 driven by RLG elements including the families Luna, Sol and Venus, the RLC family Deimos and
251 the LINE family Lucy (Figure 6E and Figure 6 - figure supplement 3A). We also found a North
252 American specific burst in DHH elements of the family Ada (increase from 4.6 to 6.1 copies on
253 average per isolate), an increase specific to Swiss populations in LINE elements, and an increase in
254 RLC elements in the Australian and the two North American populations. Analyses of complete *Z.
255 tritici* reference-quality genomes that include isolates from the Israel, Australia, Switzerland (1999)
256 and North American (1990) population revealed high TE contents in Australia and North America
257 (Oregon 1990) (Badet *et al.*, 2020). The reference-quality genomes confirmed also that the increase
258 in TEs was driven by LINE, RLG and RLC families in Australia and DHH, RLG and RLC families
259 in North America (Badet *et al.*, 2020).

260

261 TE-MEDIATED GENOME SIZE EXPANSIONS

262 The combined effects of actively copying TE families and relaxed purifying selection leads to an
263 accumulation of new TE insertions in populations. Consequently, mean genome sizes in populations
264 should increase over generations. We estimated the cumulative length of TE insertions based on the
265 length of the corresponding TE consensus sequences and found a strong increase in the total TE
266 length in populations outside the Middle East center of origin, and a second increase between the
267 two North American populations (Figure 1 - figure supplement 1). To test for incipient genome
268 expansions within the species, we first assembled genomes of all 284 isolates included in the study.
269 Given the limitations of short-read assemblies, we implemented corrective measures to compensate

270 for potential variation in assembly qualities. We corrected for variation in the GC content of
271 different sequencing datasets by downsampling reads to generate balanced sequencing read sets prior
272 to assembly (see Methods). We also excluded all reads mapping to accessory chromosomes because
273 different isolates are known to differ in the number of these chromosomes. Genome assemblies were
274 checked for completeness by retrieving the phylogenetically conserved BUSCO genes (Figure 7A).
275 Genome assemblies across different populations carry generally >99% complete BUSCO gene sets,
276 matching the completeness of reference-quality genomes of the same species (Badet *et al.*, 2020).
277 The completeness of the assemblies showed no correlation with either TE or GC content of the
278 genomes. GC content was inversely correlated with genome size consistent with the expansion of
279 repetitive regions having generally low GC content (Figure 7B). We found that the core genome size
280 varied substantially among populations with the Middle East, Australia as well as the two older
281 European and North American populations having the smallest core genome sizes (Figure 7C). We
282 found a notable increase in core genome size in both the more recent European and North American
283 populations. The increase in core genome size is positively correlated with the count and cumulative
284 length of all inserted TEs (Figure 7D, 7E and 7G) and negatively correlated with the genome-wide
285 GC content (Figure 7F and 7G). Hence, core genome size shows substantial variation within the
286 species matching the recent expansion in TEs across continents. We found the most variable genome
287 sizes in the more recent North American population (Figure 7 - figure supplement 1B). Finally, we
288 contrasted variation in genome size with the detected TE insertion dynamics. For this, we assessed
289 the variable genome segment as the difference between the smallest and largest analyzed core
290 genome. To reflect TE dynamics, we calculated the cumulative length of all detected TE insertions
291 in any given genome. We found that the cumulative length of inserted TEs represents between 4.8
292 and 184 % of the variable genome segment defined for the species or 0.2-2.6% of the estimated
293 genome size per isolate (Figure 7 - figure supplement 1C-D).

294

295 **DISCUSSION**

296 TEs play a crucial role in generating adaptive genetic variation within species but are also drivers of
297 deleterious genome expansions. We analyzed the interplay of TEs with selective and neutral
298 processes including population differentiation and incipient genome expansions. TEs have
299 substantial transposition activity in the genome but are strongly counter-selected and are maintained
300 at low frequency. TE dynamics showed distinct trajectories across populations with more recently
301 established populations having higher TE content and a concurrent expansion of the genome.

302

303 RECENT SELECTION ACTING ON TE INSERTIONS

304 TE frequencies in the species show a strong skew towards singleton insertions across populations.
305 However, our short read based analyses are possibly skewed towards over-counting singletons as
306 indicated by independent long-read mapping evaluations. Nevertheless, the skew towards low
307 frequency TE insertions indicates both that TEs are undergoing transposition and that purifying
308 selection maintains frequencies at a low level. Similar effects of selection on active TEs were
309 observed across plants and animals, including *Drosophila melanogaster* and *Brachypodium*
310 *distachyon* (Cridland *et al.*, 2013; Stritt *et al.*, 2017; Luo *et al.*, 2020). TE insertions were under-
311 represented in or near coding regions, showing a stronger purifying selection against TEs inserting
312 into genes. Coding sequences in the *Z. tritici* genome are densely packed with an average distance of
313 only ~1 kb (Goodwin *et al.*, 2011). Consistent with this high gene density, TE insertions were most
314 frequent at a distance of 200-400 bp away from coding sequences. A rapid decay in linkage
315 disequilibrium in the *Z. tritici* populations (Croll *et al.*, 2015; Hartmann *et al.*, 2018) likely
316 contributed to the efficiency of removing deleterious insertions. Some TE superfamilies have
317 preferred insertion sites in coding regions and transcription start sites (Miyao *et al.*, 2003; Fu *et al.*,
318 2013; Gilly *et al.*, 2014; Quadrana *et al.*, 2016). Hence, some heterogeneity in the observed insertion
319 site distribution across the genome is likely due to insertion preferences of individual TEs. We also
320 found evidence for positive selection acting on TEs with the strongest candidate locus being a TE
321 insertion on chromosome 12. This locus showed a frequency increase only in the more recent North

322 American population, which experienced the first systematic fungicide applications and subsequent
323 emergence of fungicide resistance in the decade prior to the last sampling (Estep *et al.*, 2015). The
324 nearest gene encodes a RTA1-like protein, a transmembrane exporter which is associated with
325 resistance towards different stressors, including antifungal compounds, and shows strong copy
326 number variation in several fungi (Soustre *et al.*, 1996; Rogers & Barker, 2003; Sirisattha *et al.*,
327 2004; Ali *et al.*, 2014; Yew *et al.*, 2016; Liang *et al.*, 2018). Hence, the TE insertion may have
328 positively modulated RTA1 expression to resist antifungals.

329 Transposition activity in a genome and counter-acting purifying selection are expected to establish
330 an equilibrium over evolutionary time (Charlesworth & Charlesworth, 1983). However, temporal
331 bursts of TE families and changes in population size due to bottlenecks or founder events are likely
332 to shift the equilibrium. Despite purifying selection, we were able to detect signatures of positive
333 selection by scanning for short-term population frequency shifts. Population genomic datasets can be
334 used to identify the most likely candidate loci underlying recent adaptation. The shallow genome-
335 wide differentiation of *Z. tritici* populations provides a powerful background to test for outlier loci
336 (Hartmann *et al.*, 2018). We found the same TE families to have experienced genome-wide copy
337 number expansions, suggesting that the availability of adaptive TE insertions may be a by-product of
338 TE bursts in individual populations.

339

340 POPULATION-LEVEL TE INVASIONS AND RELAXED SELECTION

341 Across the surveyed populations from four continents, we identified substantial variation in TE
342 counts per genome. The increase in TEs matches the global colonization history of the pathogen
343 with an increase in TE copies in more recently established populations (Zhan *et al.*, 2003;
344 Stukenbrock *et al.*, 2007). Compared to the Israeli population located nearest the center of origin in
345 the Middle East, the European populations showed a three-fold increase in TE counts. The
346 Australian and North American populations established from European descendants retained high
347 TE counts. We identified a second increase at the North American site where TE counts nearly
348 doubled again over a 25-year period. Compared to the broader increase in TEs from the Middle East,
349 the second expansion at the North American site was driven by a small subset of TE families alone.

350 Analyses of completely assembled reference-quality genomes from the same populations confirmed
351 that genome expansions were primarily driven by the same TE families belonging to the RLG, RLC
352 and DHH superfamilies (Badet *et al.*, 2020). Consistent with the contributions from individual TEs,
353 we found that the first expansion in Europe led to an increase in low-frequency variants, suggesting
354 higher transposition activity of many TEs in conjunction with strong purifying selection. The second
355 expansion at the North American site shifted TE frequencies upwards, suggesting relaxed selection
356 against TEs. The population-level context of TEs in *Z. tritici* shows how heterogeneity in TE control
357 interacts with demography to determine extant levels of TE content and, ultimately, genome size.

358

359 TE INVASION DYNAMICS UNDERPINS GENOME SIZE EXPANSIONS

360 The number of detected TEs was closely correlated with core genome size, hence genome size
361 expansions were at least partly caused by the very recent proliferation of TEs. Genome assemblies of
362 large eukaryotic genomes based on short read sequencing are often fragmented and contain chimeric
363 sequences (Nagarajan & Pop, 2013). Focusing on the less repetitive core chromosomes in the
364 genome of *Z. tritici* reduces such artefacts substantially. Because genome assemblies are the least
365 complete in the most repetitive regions, any underrepresented sequences may rather underestimate
366 than overestimate within-species variation in genome size. Hence, we consider the assembly sizes to
367 be a robust correlate of total genome size. The core genome size differences observed across the
368 species range match genome size variation typically observed among closely related species. Among
369 primates, genome size varies by ~70% with ~10% between humans and chimpanzees (Rogers &
370 Gibbs, 2014; Miga *et al.*, 2020). In fungi, genome size varies by several orders of magnitude within
371 phyla but is often highly similar among closely related species (Raffaele & Kamoun, 2012).
372 Interestingly, drastic changes in genome size have been observed in the *Blumeria* and
373 *Pseudocercospora* genera where genome size changed by 35-130% between the closest known
374 species (González-Sayer *et al.*; Frantzeskakis *et al.*, 2018). Beyond analyses of TE content variation
375 correlating with genome size evolution, proximate mechanisms driving genome expansions are
376 poorly understood. By establishing large population genetic datasets, such as those possible for crop
377 pathogens, analyses of genome size evolution become tractable at the population level.

378 TEs might not only contribute to genome expansion directly by adding length through additional
379 copies, but also by increasing the rate of chromosomal rearrangements and ectopic recombination
380 (Bourque *et al.*, 2018; Blommaert, 2020). However, TEs are not the only repetitive elements that can
381 lead to a genome size expansion. In *Arabidopsis thaliana* genomes, the 45S rDNA has been shown
382 to have the strongest impact on genome size variation, followed by 5S rDNA variation, and
383 contributions by centromeric repeats and TEs (Long *et al.*, 2013). In conjunction, recent work
384 demonstrates how repetitive sequences are drivers of genome size evolution over short evolutionary
385 timescales.

386 The activity of TEs is controlled by complex selection regimes within species. Actively transposing
387 elements may accelerate genome evolution and underpin expansions. Hence, genomic defenses
388 should evolve to efficiently target recently active TEs. Here, we show that TE activity and
389 counteracting genomic defenses have established a tenuous equilibrium across the species range. We
390 show that population subdivisions are at the origin of highly differentiated TE content within a
391 species matching genome size changes emerging over the span of only decades and centuries. In
392 conclusion, population-level analyses of genome size can recapitulate genome expansions typically
393 observed across much deeper time scales providing fundamentally new insights into genome
394 evolution.

395

396 **METHODS**

397 FUNGAL ISOLATE COLLECTION AND SEQUENCING

398 We analyzed 295 *Z. tritici* isolates covering six populations originating from four geographic
399 locations and four continents (Figure 5 - figure supplement 1), including: Middle East 1992 ($n = 30$
400 isolates, Nahal Oz, Israel), Australia 2001 ($n = 27$, Wagga Wagga), Europe 1999 ($n = 33$, Berg am
401 Irchel, Switzerland), Europe 2016 ($n = 52$, Eschikon, ca. 15km from Berg am Irchel, Switzerland),
402 North America 1990 and 2015 ($n = 56$ and $n = 97$, Willamette Valley, Oregon, United States)
403 (McDonald *et al.*, 1996; Linde *et al.*, 2002; Zhan *et al.*, 2002, 2003, 2005). Illumina short read data
404 from the Middle Eastern, Australian, European 1999 and North American 1990 populations were

405 obtained from the NCBI Sequence Read Archive (SRA) under the BioProject PRJNA327615
406 (Hartmann *et al.*, 2017). For the Switzerland 2016 and Oregon 2015 populations, asexual spores
407 were harvested from infected wheat leaves from naturally infected fields and grown in YSB liquid
408 media including 50 mgL⁻¹ kanamycin and stored in silica gel at -80°C. High-quality genomic DNA
409 was extracted from liquid cultures using the DNeasy Plant Mini Kit from Qiagen (Venlo,
410 Netherlands). The isolates were sequenced on an Illumina HiSeq in paired-end mode and raw reads
411 were deposited at the NCBI SRA under the BioProject PRJNA596434.

412

413 TE INSERTION DETECTION

414 The quality of Illumina short reads was determined with FastQC version 0.11.5
415 (<https://www.bioinformatics.babraham.ac.uk/projects/fastqc/>) (Figure 1A). To remove spuriously
416 sequenced Illumina adaptors and low quality reads, we trimmed the sequences with Trimmomatic
417 version 0.36, using the following filter parameters: illuminaclip:TruSeq3-PE-2.fa:2:30:10 leading:10
418 trailing:10 slidingwindow:5:10 minlen:50 (Bolger *et al.*, 2014). We created repeat consensus
419 sequences for TE families (sequences are available on <https://github.com/crolllab/datasets>; Figure 1 -
420 figure supplement 5) in the complete reference genome IPO323 (Goodwin *et al.*, 2011) with
421 RepeatModeler version open-4.0.7 (<http://www.repeatmasker.org/RepeatModeler/>) based on the
422 RepBase Sequence Database and de novo (Bao *et al.*, 2015). TE classification into superfamilies and
423 families was based on an approach combining detection of conserved protein sequences and tools to
424 detect non-autonomous TEs (Badet *et al.*, 2020). To detect TE insertions, we used the R-based tool
425 `ngs_te_mapper` version 79ef861f1d52cdd08eb2d51f145223fad0b2363c integrated into the
426 McClintock pipeline version 20cb912497394fabddcdaa175402adacf5130bd1, using `bwa` version
427 0.7.4-r385 to map Illumina short reads, `samtools` version 0.1.19 to convert alignment file formats
428 and R version 3.2.3 (Li & Durbin, 2009; Li *et al.*, 2009; Linheiro & Bergman, 2012; R Core Team,
429 2017; Nelson *et al.*, 2017).

430

431 DOWN-SAMPLING ANALYSIS

432 We performed a down-sampling analysis to estimate the sensitivity of the TE detection with
433 `ngs_te_mapper` based on variation in read depth. We selected one isolate per population matching
434 the average coverage of the population. We extracted the per-base pair read depth with the
435 `genomecov` function of `bedtools` version 2.27.1 and calculated the genome-wide mean read depth
436 (Quinlan & Hall, 2010). The number of reads in the original fastq file was reduced in steps of 10%
437 to simulate the impact of reduced coverage. We analyzed each of the obtained reduced read subsets
438 with `ngs_te_mapper` using the same parameters as described above. The correlation between the
439 number of detected insertions and the read depth was visualized using the function `nls` with model
440 `SSlogis` in R and visualized with `ggplot2` (Wickham, 2016). The number of detected TEs increased
441 with the number of reads until reaching a plateau indicating saturation (Figure 1B). Saturation was
442 reached at a coverage of approximately 15X, hence we retained only isolates with an average read
443 depth above 15X for further analyses. We thus excluded one isolate from the Oregon 2015
444 population and ten isolates from the Switzerland 2016 population.

445

446 VALIDATION PROCEDURE FOR PREDICTED TE INSERTIONS

447 `ngs_te_mapper` detects the presence but not the absence of a TE at any given locus. We devised
448 additional validation steps to ascertain both the presence as well as the absence of a TE across all
449 loci in all individuals. TEs absent in the reference genome were validated by re-analyzing mapped
450 Illumina reads. Reads spanning both parts of a TE sequence and an adjacent chromosomal sequence
451 should only map to the reference genome sequence and cover the target site duplication of the TE
452 (Figure 1C). We used `bowtie2` version 2.3.0 with the parameter `--very-sensitive-local` to map
453 Illumina short reads of each isolate on the reference genome IPO323 (Langmead & Salzberg, 2012).
454 Mapped Illumina short reads were then sorted and indexed with `samtools` and the resulting bam file
455 was converted to a bed file with the function `bamtobed` in `bedtools`. We extracted all mapped reads
456 with an end point located within 100 bp of the target site duplication (Figure 1C). We tested whether
457 the number of reads with a mapped end around the target site duplication significantly deviated if the
458 mapping ended exactly at the boundary. A mapped read ending exactly at the target site duplication

459 boundary is indicative of a split read mapping to a TE sequence absent in the reference genome. To
460 test for the deviation in the number of read mappings around the target site duplication, we used a
461 Poisson distribution and the *ppois* function in R version 3.5.1 (Figure 1C). We identified a TE as
462 present in an isolate if tests on either side of the target site duplication had a *p*-value < 0.001 (Figure
463 5 - figure supplement 1; Figure 1 - figure supplement 1B and Figure 1 - figure supplement 2).

464

465 For TEs present in the reference genome, we analyzed evidence for spliced junction reads spanning
466 the region containing the TE. Spliced reads are indicative of a discontinuous sequence and, hence,
467 absence of the TE in a particular isolate (Figure 1D). We used STAR version 2.5.3a to detect spliced
468 junction reads with the following set of parameters: `--runThreadN 1 --outFilterMultimapNmax 100 -`
469 `--winAnchorMultimapNmax 200 --outSAMmultNmax 100 --outSAMtype BAM Unsorted --`
470 `outFilterMismatchNmax 5 --alignIntronMin 150 --alignIntronMax 15000` (Dobin *et al.*, 2012). We
471 then sorted and indexed the resulting bam file with samtools and converted split junction reads with
472 the function `bam2hints` in bamtools version 2.5.1 (Barnett *et al.*, 2011). We selected loci without
473 overlapping spliced junction reads using the function `intersect` in bedtools with the parameter `-loj -v`.
474 We considered a TE as truly absent in an isolate if `ngs_te_mapper` did not detect a TE and evidence
475 for spliced junction reads were found, indicating that the isolate had no inserted TE in this region. If
476 the absence of a TE could not be confirmed by spliced junction reads, we labelled the genotype as
477 missing. Finally, we excluded TE loci with more than 20% missing data from further investigations
478 (Figure 1D and Figure 1 - figure supplement 1C).

479

480 CLUSTERING OF TE INSERTIONS INTO LOCI

481 We identified insertions across isolates as being the same locus if all detected TEs belonged to the
482 same TE family and insertion sites differed by ≤ 100 bp (Figure 1 - figure supplement 3). We used
483 the R package *GenomicRanges* version 1.28.6 with the functions `makeGRangesFromDataFrame` and
484 `findOverlaps` and the R package *devtools* version 1.13.4 (Lawrence *et al.*, 2013; Wickham & Chang,
485 2016). We used the R package *dplyr* version 0.7.4 to summarize datasets
486 (<https://dplyr.tidyverse.org/>). Population-specific frequencies of insertions were calculated with the

487 function `allele.count` in the R package *hierfstat* version 0.4.22 (Goudet, 2005). We conducted a
488 principal component analysis for TE insertion frequencies filtering for a minor allele frequency \geq
489 5%. We also performed a principal component analysis for genome-wide single nucleotide
490 polymorphism (SNP) data obtained from Hartmann et al (2017) and Singh et al (2020). As described
491 previously, SNPs were hard-filtered with VariantFiltration and SelectVariants tools integrated in the
492 Genome Analysis Toolkit (GATK) (McKenna *et al.*, 2010). SNPs were removed if any of the
493 following filter conditions applied: `QUAL<250; QD<20.0; MQ<30.0; -2 > BaseQRankSum > 2; -2`
494 `> MQRankSum > 2; -2 > ReadPosRankSum > 2; FS>0.1`. SNPs were excluded with `vcftools` version
495 0.1.17 and `plink` version 1.9 requiring a genotyping rate $>90\%$ and a minor allele frequency $>5\%$
496 (<https://www.cog-genomics.org/plink2>, Chang et al., 2015). Finally, we converted tri-allelic SNPs to
497 bi-allelic SNPs by recoding the least frequent allele as a missing genotype. Principal component
498 analysis was performed using the *gdsfmt* and *SNPRelate* packages in R (Zheng *et al.*, 2012, 2017).
499 For a second principal component analysis with a reduced set of random markers, we randomly
500 selected SNPs with `vcftools` and the following set of parameters: `--maf 0.05 --thin 200000` to obtain
501 an approximately equivalent number of SNPs as TE loci.

502

503 EVALUATION OF SINGLETON INSERTIONS

504 To evaluate the reliability of singleton TE insertion loci, we analyzed singleton loci in isolates for
505 which we had both Illumina datasets and complete reference-quality genomes (Badet *et al.*, 2020).
506 From a set of 19 long-read PacBio reference genomes spanning the global distribution of *Z. tritici*,
507 one isolate each from Australia, Israel, North America (1990) and four isolates from Europe (1999)
508 were also included in the TE insertion screening. To assess the reliability of singleton TE insertions,
509 we first investigated structural variation analyses among the reference genomes (Badet *et al.*, 2021,
510 Supplementary Data 1 and 2). The structural variation was called both based on split read mapping
511 of PacBio reads and pairwise whole-genome alignments. Using `bedtools intersect`, we recovered for
512 the 31 singleton TE loci in the 7 analyzed genomes a total of 17 loci showing either an indel,
513 translocation, copy number polymorphism, duplication, inverted duplication, inversion, or inverted

514 translocation at the same location. We visually inspected the PacBio read alignment bam files
515 against the IPO323 reference genome using IGV version 2.4.16 (Robinson *et al.*, 2011), and found a
516 typical coverage increase at the target site duplication, with most read mappings interrupted at the
517 target site duplication as expected for an inserted TE. For the 14 remaining TE loci, we extracted the
518 region of the predicted insertion and padded the sequence on both ends with an additional 500 bp
519 using samtools faidx. We used blast to identify a homologous region in the assembled reference-
520 quality genomes. Matching regions were inspected based on blastn for the presence of a TE
521 sequence matching the TE family originally detected at the locus. With this second approach, we
522 confirmed an additional five singletons to be true insertions. Both methods combined produced
523 supportive evidence for 22 out of 31 singleton insertions (71%). We calculated the read coverage
524 after mapping to the reference genome IPO323 with bedtools genomecov for each PacBio long-read
525 dataset and calculated mean coverage for 500 bp regions around singleton TE insertions.

526

527 POPULATION DIFFERENTIATION IN TE FREQUENCIES

528 We calculated Nei's fixation index (F_{ST}) between pairs of populations using the R packages *hierfstat*
529 and *adegenet* version 2.1.0 (Jombart, 2008; Jombart & Ahmed, 2011). To understand the
530 chromosomal context of TE insertion loci across isolates, we analyzed draft genome assemblies. We
531 generated *de novo* genome assemblies for all isolates using SPAdes version 3.5.0 with the parameter
532 --careful and a kmer range of "21, 29, 37, 45, 53, 61, 79, 87" (Bankevich *et al.*, 2012). We used
533 blastn to locate genes adjacent to TE insertion loci on genomic scaffolds of each isolate. We then
534 extracted scaffold sequences surrounding 10 kb up- and downstream of the localized gene with the
535 function faidx in samtools and reverse complemented the sequence if needed. Then, we performed
536 multiple sequence alignments for each locus across all isolates with MAFFT version 7.407 with
537 parameter --maxiterate 1000 (Katoh & Standley, 2013). We performed visual inspections to ensure
538 correct alignments across isolates using Jalview version 2.10.5 (Waterhouse *et al.*, 2009). To
539 generate phylogenetic trees of individual gene or TE loci, we extracted specific sections of the
540 alignment using the function extractalign in EMBOSS version 6.6.0 (Rice *et al.*, 2000) and
541 converted the multiple sequence alignment into PHYLIP format with jmodeltest version 2.1.10 using

542 the `-getPhyIip` parameter. We then estimated maximum likelihood phylogenetic trees with the
543 software PhyML version 3.0, the K80 substitution model and 100 bootstraps on the ATGC South of
544 France bioinformatics platform (Guindon & Gascuel, 2003; Guindon *et al.*, 2010; Darriba *et al.*,
545 2012). Bifurcations with a supporting value lower than 10% were collapsed in TreeGraph version
546 2.15.0-887 beta and trees were visualized as circular phylograms in Dendroscope version 2.7.4
547 (Huson *et al.*, 2007; Stöver & Müller, 2010). For loci showing complex rearrangements, we
548 generated synteny plots using 19 completely sequenced genomes from the same species using the R
549 package *genoplotR* version 0.8.9 (Guy *et al.*, 2010; Badet *et al.*, 2020). We calculated the
550 population-specific allele frequency for TE loci and estimated the exponential decay curve with a
551 self-starting Nls asymptomatic regression model `nls(p_loci ~ SSasymp(p_round, Asym, R0, lrc)` in
552 R.

553 We analyzed signatures of selective sweeps based on genome-wide SNPs using the extended
554 haplotype homozygosity (EHH) tests implemented in the R package *REHH* (Sabeti *et al.*, 2007;
555 Gautier & Vitalis, 2012). We analyzed within-population signatures based on the *iHS* statistic and
556 chose a maximum gap distance of 20 kb. We also analyzed cross-population signatures based on the
557 XP-EHH statistic for the following two population pairs: North America 1990 versus North America
558 2015, Europe 1999 versus Europe 2016. We defined significant selective sweeps as being among the
559 99.9th percentile outliers of the *iHS* and XP-EHH statistics. Significant SNPs at less than 5 kb were
560 clustered into a single selective sweep region adding ± 2.5 kb. Finally, we analyzed whether TE
561 loci in the population pairs were within 10 kb of a region identified as a selective sweep by XP-EHH
562 using the function `intersect` from *bedtools*.

563

564 GENOMIC LOCATION OF TE INSERTIONS

565 To characterize the genomic environment of TE insertion loci, we split the reference genome into
566 non-overlapping windows of 10 kb using the function `splitter` from *EMBOSS*. TEs were located in
567 the reference genome using *RepeatMasker* providing consensus sequences from *RepeatModeler*
568 (<http://www.repeatmasker.org/>). To analyze coding sequence, we retrieved the gene annotation for

569 the reference genome (Grandaubert *et al.*, 2015). We estimated the percentage covered by genes or
570 TEs per window using the function `intersect` in `bedtools`. Additionally, we calculated the GC content
571 using the tool `get_gc_content` ([https://github.com/spundhir/RNA-](https://github.com/spundhir/RNA-Seq/blob/master/get_gc_content.pl)
572 [Seq/blob/master/get_gc_content.pl](https://github.com/spundhir/RNA-Seq/blob/master/get_gc_content.pl)). We extracted the number of TEs present in 1 kb windows
573 around each annotated core gene in the reference genome IPO323, using the function `window` in
574 `bedtools`. We calculated the relative distances between each gene and the closest TE with the
575 function `bedtools closest`. For the TEs inserted into genes, we used the function `intersect` in `bedtools`
576 to distinguish intron and exon insertions with the parameters `-wo` and `-v`, respectively. TEs that
577 overlap more than one exon were only counted once. For each 100 bp segment in the 1 kb windows
578 as well as for introns and exons, we calculated the mean number of observed TE insertions per base
579 pair. We calculated the mean number of TEs per window and calculated the \log_2 of the observed
580 number of TE insertions divided by the expected value. We extracted information about
581 recombination hotspots from Croll *et al.* (2015). This dataset is based on two experimental crosses
582 initiated from isolates included in our analyses (1A5x1E4, 3D1x3D7). The recombination rates were
583 assessed based on the reference genome IPO323 and analyzed with the *R/qtl* package in R. We used
584 `bedtools intersect` to compare both TE density in IPO323 and TE insertion polymorphism with
585 predicted recombination hotspots.

586

587 CORE GENOME SIZE ESTIMATION

588 Accessory chromosomes show presence/absence variation within the species and length
589 polymorphism (Goodwin *et al.*, 2011; Croll *et al.*, 2013) and thus impact genome size. We
590 controlled for this effect by first mapping sequencing reads to the reference genome IPO323 using
591 `bowtie2` with `--very-sensitive-local` settings and retained only reads mapping to any of the 13 core
592 chromosomes using `seqtk subseq v1.3-r106` (<https://github.com/lh3/seqtk/>). Furthermore, we found
593 that different sequencing runs showed minor variation in the distribution of the per read GC content.
594 In particular, reads of a GC content lower than 30 % were underrepresented in the Australian (mean
595 reads < 30 % of the total readset: 0.05 %), North American 1990 (0.07 %) and Middle East (0.1 %)
596 populations, and higher in the Europe 1999 (1.3 %), North American 2015 (3.0 %) and Europe 2016

597 (4.02 %) populations (Figure 1 - figure supplement 4). Library preparation protocols and Illumina
598 sequencer generations are known factors influencing the recovery of reads of varying GC content
599 (Benjamini & Speed, 2012).

600

601 To control a potential bias stemming from this, we subsampled reads based on GC content to create
602 homogeneous datasets. For this, we first retrieved the mean GC content for each read pair using
603 geecee in EMBOSS and binned reads according to GC content. For the bins with a GC content
604 <30%, we calculated the mean proportion of reads from the genome over all samples. We then used
605 seqtk subseq to subsample reads of <30% to adjust the mean GC content among readsets. We
606 generated *de novo* genome assemblies using the SPAdes assembler version with the parameters --
607 careful and a kmer range of “21, 29, 37, 45, 53, 61, 79, 87”. The SPAdes assembler is optimized for
608 the assembly of relatively small eukaryotic genomes. We evaluated the completeness of the
609 assemblies using BUSCO v4.1.1 with the fungi_odb10 gene test set (Simão *et al.*, 2015). We finally
610 ran Quast v5.0.2 to retrieve assembly metrics including scaffolds of at least 1 kb (Mikheenko *et al.*,
611 2018).

612

613 FUNGICIDE RESISTANCE ASSAY

614 To quantify susceptibility towards propiconazole we used a previously published microtiter plate
615 assay dataset with 3 replicates performed for each isolate and concentration. Optical density was
616 used to estimate growth rates under different fungicide concentrations (0, 0.00006, 0.00017, 0.0051,
617 0.0086, 0.015, 0.025, 0.042, 0.072, 0.20, 0.55, 1.5 mgL⁻¹) (Hartmann *et al.*, 2020). We calculated
618 dose-response curves and estimated the half-maximal lethal concentration EC₅₀ with a 4-parameter
619 logistics curve in the R package *drc* (Ritz & Streibig, 2005).

620

621 **Data availability**

622 Sequence data is deposited at the NCBI SRA under the accession numbers PRJNA327615,
623 PRJNA596434 and PRJNA178194. Transposable element consensus sequences are available from
624 <https://github.com/crolllab/datasets>.

625

626 **Author contributions**

627 UO and DC conceived the study, UO, TW and DC designed analyses, UO, TB, TV and FEH
628 performed analyses, FEH, NKS, LNA, PK, CCM and BAM provided samples/datasets, BAM and
629 DC provided funding, UO and DC wrote the manuscript with input from co-authors. All authors
630 reviewed the manuscript and agreed on submission.

631

632 **Acknowledgments**

633 We thank Andrea Sánchez Vallet, Anne C. Roulin, Luzia Stalder, Adam Taranto, Emilie Chanclud
634 and Alice Feurtey for helpful discussions and comments on previous versions of the manuscript. We
635 also thank the three reviewers for very helpful suggestions. We thank C. Sarai Reyes-Avila for
636 advice on statistical analyses. DC is supported by the Swiss National Science (grants
637 31003A_173265) and the Fondation Pierre Mercier pour la Science.

638

639 **Competing interests**

640 We declare to have no competing interests.

641

642

643 **REFERENCES**

- 644 **Ali SS, Khan M, Mullins E, Doohan FM. 2014.** Identification of *Fusarium oxysporum* Genes
645 Associated with Lignocellulose Bioconversion Competency. *Bioenergy Research* **7**: 110–119.
- 646 **Badet T, Fouché S, Hartmann FE, Zala M, Croll D. 2021.** Machine-learning predicts genomic
647 determinants of meiosis-driven structural variation in a eukaryotic pathogen. *Nature*
648 *Communications* **12**.
- 649 **Badet T, Oggenfuss U, Abraham L, McDonald BA, Croll D. 2020.** A 19-isolate reference-quality
650 global pangenome for the fungal wheat pathogen *Zymoseptoria tritici*. *BMC Biology* **18**: 12.
- 651 **Bankevich A, Nurk S, Antipov D, Gurevich AA, Dvorkin M, Kulikov AS, Lesin VM,**
652 **Nikolenko SI, Pham S, Prjibelski AD, et al. 2012.** SPAdes: a new genome assembly algorithm and

- 653 its applications to single-cell sequencing. *Journal of computational biology*: a journal of
654 *computational molecular cell biology* **19**: 455–77.
- 655 **Bao W, Kojima KK, Kohany O. 2015.** Repbase Update, a database of repetitive elements in
656 eukaryotic genomes. *Mobile DNA* **6**: 4–9.
- 657 **Barnett DW, Garrison EK, Quinlan AR, Strömberg MP, Marth GT. 2011.** Bamtools: A C++
658 API and toolkit for analyzing and managing BAM files. *Bioinformatics* **27**: 1691–1692.
- 659 **Baucom RS, Estill JC, Leebens-Mack J, Bennetzen JL. 2008.** Natural selection on gene function
660 drives the evolution of LTR retrotransposon families in the rice genome. *Genome Research* **19**: 243–
661 254.
- 662 **Benjamini Y, Speed TP. 2012.** Summarizing and correcting the GC content bias in high-throughput
663 sequencing. *Nucleic Acids Research* **40**: 1–14.
- 664 **Blommaert J. 2020.** Genome size evolution: towards new model systems for old questions.
665 *Proceedings. Biological sciences* **287**: 20201441.
- 666 **Bolger AM, Lohse M, Usadel B. 2014.** Trimmomatic: a flexible trimmer for Illumina sequence
667 data. *Bioinformatics* **30**: 2114–2120.
- 668 **Bonifacino JS, Glick BS. 2004.** The Mechanisms of Vesicle Budding and Fusion. *Cell* **116**: 153–
669 166.
- 670 **Bourque G, Burns KH, Gehring M, Gorbunova V, Seluanov A, Hammell M, Imbeault M,
671 Izsvák Z, Levin HL, Macfarlan TS, et al. 2018.** Ten things you should know about transposable
672 elements. *Genome Biology* **19**: 199.
- 673 **Charlesworth B, Charlesworth D. 1983.** The population dynamics of transposable elements.
674 *Genetical Research* **42**: 1–27.
- 675 **Chuong EB, Elde NC, Feschotte C. 2017.** Regulatory activities of transposable elements: from
676 conflicts to benefits. *Nature Reviews Genetics* **18**: 71–86.
- 677 **Cridland JM, Macdonald SJ, Long AD, Thornton KR. 2013.** Abundance and distribution of
678 transposable elements in two drosophila QTL mapping resources. *Molecular Biology and Evolution*
679 **30**: 2311–2327.
- 680 **Croll D, Lendenmann MH, Stewart E, McDonald BA. 2015.** The Impact of Recombination
681 Hotspots on Genome Evolution of a Fungal Plant Pathogen. *Genetics* **201**: 1213-U787.
- 682 **Croll D, Zala M, McDonald BA. 2013.** Breakage–fusion–bridge Cycles and Large Insertions
683 Contribute to the Rapid Evolution of Accessory Chromosomes in a Fungal Pathogen (J Heitman,
684 Ed.). *PLOS Genetics* **9**: e1003567.
- 685 **Darriba D, Taboada GL, Doallo R, Posada D. 2012.** jModelTest 2: more models, new heuristics
686 and parallel computing. *Nature Methods* **9**: 772.
- 687 **Dobin A, Davis CA, Schlesinger F, Drenkow J, Zaleski C, Jha S, Gingeras TR, Batut P,
688 Chaisson M. 2012.** STAR: ultrafast universal RNA-seq aligner. *Bioinformatics* **29**: 15–21.
- 689 **Eichler EE, Sankoff D. 2003.** Structural dynamics of eukaryotic chromosome evolution. *Science*
690 **301**: 793–797.
- 691 **Estep LK, Torriani SFF, Zala M, Anderson NP, Flowers MD, McDonald BA, Mundt CC,
692 Brunner PC. 2015.** Emergence and early evolution of fungicide resistance in North American
693 populations of *Zymoseptoria tritici*. *Plant Pathology* **64**: 961–971.
- 694 **Feschotte C. 2008.** Transposable elements and the evolution of regulatory networks. *Nature*
695 *Reviews Genetics* **9**: 397–405.
- 696 **Feurtay A, Lorrain C, Croll D, Eschenbrenner C, Freitag M, Habig M, Haueisen J, Möller M,
697 Schotanus K, Stukenbrock EH. 2020.** Genome compartmentalization predates species divergence
698 in the plant pathogen genus *Zymoseptoria*. *BMC genomics* **21**: 588.
- 699 **Fouché S, Badet T, Oggenfuss U, Plissonneau C, Francisco CS, Croll D. 2019.** Stress-driven
700 transposable element de-repression dynamics in a fungal pathogen. *Molecular Biology and*
701 *Evolution*.
- 702 **Frantzeskakis L, Kracher B, Kusch S, Yoshikawa-Maekawa M, Bauer S, Pedersen C, Spanu**

- 703 **PD, Maekawa T, Schulze-Lefert P, Panstruga R. 2018.** Signatures of host specialization and
704 recent transposable element burst in the dynamic one-speed genome of the fungal barley powdery
705 mildew pathogen. *BMC Genomics* **19**: 1–23.
- 706 **Fu Y, Kawabe A, Etcheverry M, Ito T, Toyoda A, Fujiyama A, Colot V, Tarutani Y, Kakutani**
707 **T. 2013.** Mobilization of a plant transposon by expression of the transposon-encoded anti-silencing
708 factor. *EMBO Journal* **32**: 2407–2417.
- 709 **Gautier M, Vitalis R. 2012.** Rehh An R package to detect footprints of selection in genome-wide
710 SNP data from haplotype structure. *Bioinformatics* **28**: 1176–1177.
- 711 **Gilly A, Etcheverry M, Madoui MA, Guy J, Quadrana L, Alberti A, Martin A, Heitkam T,**
712 **Engelen S, Labadie K, et al. 2014.** TE-Tracker: systematic identification of transposition events
713 through whole-genome resequencing. *Bmc Bioinformatics* **15**.
- 714 **González-Sayer S, Oggenfuss U, García I, Aristizabal F.** High-quality genome assembly of
715 *Pseudocercospora ulei* the main threat to natural rubber trees. : 0–1.
- 716 **Goodwin SB, Ben M'Barek S, Dhillon B, Wittenberg AHJ, Crane CF, Hane JK, Foster AJ,**
717 **Van der Lee TAJ, Grimwood J, Aerts A, et al. 2011.** Finished Genome of the Fungal Wheat
718 Pathogen *Mycosphaerella graminicola* Reveals Dispensome Structure, Chromosome Plasticity, and
719 Stealth Pathogenesis (HS Malik, Ed.). *PLOS Genetics* **7**: e1002070.
- 720 **Goudet J. 2005.** Hierstat, a package for R to compute and test heirarchical F-statistics. *Molecular*
721 *Ecology Notes* **5**: 184–186.
- 722 **Grandaubert J, Bhattacharyya A, Stukenbrock EH. 2015.** RNA-seq-Based Gene Annotation and
723 Comparative Genomics of Four Fungal Grass Pathogens in the Genus *Zymoseptoria* Identify Novel
724 Orphan Genes and Species-Specific Invasions of Transposable Elements. *G3-Genes Genomes*
725 *Genetics* **5**: 1323–1333.
- 726 **Guindon S, Dufayard J-F, Lefort V, Anisimova M, Hordijk W, Gascuel O. 2010.** New
727 Algorithms and Methods to Estimate Maximum-Likelihood Phylogenies: Assessing the Performance
728 of PhyML 3.0. *Systematic Biology* **59**: 307–321.
- 729 **Guindon S, Gascuel O. 2003.** A simple, fast, and accurate algorithm to estimate large phylogenies
730 by maximum likelihood. *Systematic Biology* **52**: 696–704.
- 731 **Guy L, Kultima JR, Andersson SGE. 2010.** GenoPlotR: comparative gene and genome
732 visualization in R. *Bioinformatics* **26**: 2334–2335.
- 733 **Hartmann F, Croll D. 2017.** Distinct Trajectories of Massive Recent Gene Gains and Losses in
734 Populations of a Microbial Eukaryotic Pathogen. *Molecular Biology and Evolution*.
- 735 **Hartmann F, McDonald M, Croll D. 2018.** Genome-wide evidence for divergent selection
736 between populations of a major agricultural pathogen. *Molecular Ecology* **27**: 2725–2741.
- 737 **Hartmann FE, Sánchez-Vallet A, McDonald BA, Croll D. 2017.** A fungal wheat pathogen
738 evolved host specialization by extensive chromosomal rearrangements. *The ISME Journal* **11**: 1189–
739 1204.
- 740 **Hartmann FE, Vonlanthen T, Singh NK, McDonald MC, Milgate A, Croll D. 2020.** The
741 complex genomic basis of rapid convergent adaptation to pesticides across continents in a fungal
742 plant pathogen. *Molecular Ecology*.
- 743 **Hollister JD, Gaut BS. 2009.** Epigenetic silencing of transposable elements: A trade-off between
744 reduced transposition and deleterious effects on neighboring gene expression. *Genome Research* **19**:
745 1419–1428.
- 746 **Huson DH, Richter DC, Rausch C, DeZulian T, Franz M, Rupp R. 2007.** Dendroscope: An
747 interactive viewer for large phylogenetic trees. *BMC Bioinformatics* **8**: 1–6.
- 748 **Jiao W-B, Schneeberger K. 2019.** Chromosome-level assemblies of multiple *Arabidopsis thaliana*
749 accessions reveal hotspots of genomic rearrangements. *bioRxiv*: 738880.
- 750 **Jombart T. 2008.** Adegenet: A R package for the multivariate analysis of genetic markers.
751 *Bioinformatics* **24**: 1403–1405.
- 752 **Jombart T, Ahmed I. 2011.** adegenet 1.3-1: New tools for the analysis of genome-wide SNP data.

- 753 *Bioinformatics* **27**: 3070–3071.
- 754 **Katoh K, Standley DM. 2013.** MAFFT multiple sequence alignment software version 7:
755 Improvements in performance and usability. *Molecular Biology and Evolution* **30**: 772–780.
- 756 **Kidwell MG. 2002.** Transposable elements and the evolution of genome size in eukaryotes.
757 *Genetica* **115**: 49–63.
- 758 **Krishnan P, Meile L, Plissonneau C, Ma X, Hartmann FE, Croll D, McDonald BA, Sánchez-**
759 **Vallet A. 2018.** Transposable element insertions shape gene regulation and melanin production in a
760 fungal pathogen of wheat. *BMC Biology* **16**: 1–18.
- 761 **Lai X, Schnable JC, Liao Z, Xu J, Zhang G, Li C, Hu E, Rong T, Xu Y, Lu Y. 2017.** Genome-
762 wide characterization of non-reference transposable element insertion polymorphisms reveals
763 genetic diversity in tropical and temperate maize. *BMC Genomics* **18**: 1–13.
- 764 **Langmead B, Salzberg SL. 2012.** Fast gapped-read alignment with Bowtie 2. *Nature Methods* **9**:
765 357–359.
- 766 **Lawrence M, Huber W, Pagès H, Aboyoun P, Carlson M, Gentleman R, Morgan MT, Carey**
767 **VJ. 2013.** Software for Computing and Annotating Genomic Ranges (A Prlic, Ed.). *PLOS*
768 *Computational Biology* **9**: e1003118.
- 769 **Li H, Durbin R. 2009.** Fast and accurate short read alignment with Burrows-Wheeler transform.
770 *Bioinformatics* **25**: 1754–1760.
- 771 **Li H, Handsaker B, Wysoker A, Fennell T, Ruan J, Homer N, Marth G, Abecasis G, Durbin R.**
772 **2009.** The Sequence Alignment/Map format and SAMtools. *Bioinformatics* **25**: 2078–2079.
- 773 **Liang X, Wang B, Dong Q, Li L, Rollins JA, Zhang R, Sun G. 2018.** Pathogenic adaptations of
774 *Colletotrichum* fungi revealed by genome wide gene family evolutionary analyses. *PLoS ONE* **13**:
775 1–25.
- 776 **Lim JK. 1988.** Intrachromosomal rearrangements mediated by hobo transposons in *Drosophila*
777 *melanogaster*. *PNAS* **85**: 9153–9157.
- 778 **Linde CC, Zhan J, McDonald BA. 2002.** Population Structure of *Mycosphaerella graminicola* □:
779 From Lesions to Continents. *Phytopathology* **92**: 946–955.
- 780 **Linheiro RS, Bergman CM. 2012.** Whole Genome Resequencing Reveals Natural Target Site
781 Preferences of Transposable Elements in *Drosophila melanogaster* (JE Stajich, Ed.). *PLOS ONE* **7**:
782 e30008.
- 783 **Long Q, Rabanal FA, Meng D, Huber CD, Farlow A, Platzer A, Zhang Q, Vilhjálmsson BJ,**
784 **Korte A, Nizhynska V, et al. 2013.** Massive genomic variation and strong selection in *Arabidopsis*
785 *thaliana* lines from Sweden. *Nature Genetics* **45**: 884–890.
- 786 **Lu L, Chen J, Robb SMC, Okumoto Y, Stajich JE, Wessler SR. 2017.** Tracking the genome-
787 wide outcomes of a transposable element burst over decades of amplification. *Proceedings of the*
788 *National Academy of Sciences*: 201716459.
- 789 **Luo S, Zhang H, Duan Y, Yao X, Clark AG, Lu J. 2020.** The evolutionary arms race between
790 transposable elements and piRNAs in *Drosophila melanogaster*. *BMC Evolutionary Biology* **20**: 14.
- 791 **Lynch M. 2007.** *The Origins of Genome Architecture*. Sunderland MA: Sinauer Associates.
- 792 **McDonald BA, Mundt CC, Chen R. 1996.** The role of selection on the genetic structure of
793 pathogen populations □: Evidence from field experiments with *Mycosphaerella graminicola* on
794 wheat. *Euphytica* **92**: 73–80.
- 795 **McKenna A, Hanna M, Banks E, Sivachenko A, Cibulskis K, Kernytzky A, Garimella K,**
796 **Altshuler D, Gabriel S, Daly M, et al. 2010.** The Genome Analysis Toolkit: A MapReduce
797 framework for analyzing next-generation DNA sequencing data. *Genome Research* **20**: 1297–1303.
- 798 **Meile L, Croll D, Brunner PC, Plissonneau C, Hartmann FE, McDonald BA, Sánchez-Vallet**
799 **A. 2018.** A fungal avirulence factor encoded in a highly plastic genomic region triggers partial
800 resistance to septoria tritici blotch. *New Phytologist* **219**: 1048–1061.
- 801 **Miga KH, Koren S, Rhie A, Vollger MR, Gershman A, Bzikadze A, Brooks S, Howe E,**
802 **Porubsky D, Logsdon GA, et al. 2020.** Telomere-to-telomere assembly of a complete human X

- 803 chromosome. *Nature* **585**: 79–84.
- 804 **Mikheenko A, Prjibelski A, Saveliev V, Antipov D, Gurevich A. 2018.** Versatile genome
805 assembly evaluation with QUASt-LG. *Bioinformatics* **34**: i142–i150.
- 806 **Miyao A, Tanaka K, Murata K, Sawaki H, Takeda S, Abe K, Shinozuka Y, Onosato K,**
807 **Hirochika H. 2003.** Target site specificity of the Tos17 retrotransposon shows a preference for
808 insertion within genes and against insertion in retrotransposon-rich regions of the genome. *Plant*
809 *Cell* **15**: 1771–1780.
- 810 **Nagarajan N, Pop M. 2013.** Sequence assembly demystified. *Nature Reviews Genetics* **14**: 157–
811 167.
- 812 **Nakamura K, Oshima T, Morimoto T, Ikeda S, Yoshikawa H, Shiwa Y, Ishikawa S, Linak**
813 **MC, Hirai A, Takahashi H, et al. 2011.** Sequence-specific error profile of Illumina sequencers.
814 *Nucleic Acids Research* **39**.
- 815 **Nelson MG, Linheiro RS, Bergman CM. 2017.** McClintock: An Integrated Pipeline for Detecting
816 Transposable Element Insertions in Whole-Genome Shotgun Sequencing Data. *G3:*
817 *Genes/Genomes/Genetics* **7**: 2763–2778.
- 818 **Oliver KR, McComb JA, Greene WK. 2013.** Transposable elements: Powerful contributors to
819 angiosperm evolution and diversity. *Genome Biology and Evolution* **5**: 1886–1901.
- 820 **Omrane S, Audéon C, Ignace A, Duplaix C, Aouini L, Kema G, Walker A-S, Fillinger S. 2017.**
821 Plasticity of the MFS1 promoter leads to multi drug resistance in the wheat pathogen *Zymoseptoria*
822 *tritici*. *mSphere*: 1–42.
- 823 **Omrane S, Sghyer H, Audeon C, Lanen C, Duplaix C, Walker AS, Fillinger S. 2015.** Fungicide
824 efflux and the MgMFS1 transporter contribute to the multidrug resistance phenotype in
825 *Zymoseptoria tritici* field isolates. *Environmental Microbiology* **17**: 2805–2823.
- 826 **Peter M, Kohler A, Ohm RA, Kuo A, Krützmann J, Morin E, Arend M, Barry KW, Binder M,**
827 **Choi C, et al. 2016.** Ectomycorrhizal ecology is imprinted in the genome of the dominant symbiotic
828 fungus *Cenococcum geophilum*. *Nature Communications* **7**: 1–15.
- 829 **Petrov DA, Aminetzach YT, Davis JC, Bensasson D, Hirsh AE. 2003.** Size matters: Non-LTR
830 retrotransposable elements and ectopic recombination in *Drosophila*. *Molecular Biology and*
831 *Evolution* **20**: 880–892.
- 832 **Piegu B, Guyot R, Picault N, Roulin A, Sanyal A, Kim H, Collura K, Brar DS, Jackson S,**
833 **Wing RA, et al. 2006.** Doubling genome size without polyploidization: Dynamics of
834 retrotransposition-driven genomic expansions in *Oryza australiensis*, a wild relative of rice. *Genome*
835 *Research* **21**: 1201.
- 836 **Plissonneau C, Stürchler A, Croll D. 2016.** The Evolution of Orphan Regions in Genomes of a
837 Fungal Pathogen of Wheat. *mBio* **7**: 1–13.
- 838 **Quadrana L, Silveira AB, Mayhew GF, LeBlanc C, Martienssen RA, Jeddelloh JA, Colot V.**
839 **2016.** The *Arabidopsis thaliana* mobilome and its impact at the species level. *Elife* **5**.
- 840 **Quinlan AR, Hall IM. 2010.** BEDTools: A flexible suite of utilities for comparing genomic
841 features. *Bioinformatics* **26**: 841–842.
- 842 **R Core Team. 2017.** R: A language and environment for statistical computing. R Foundation for
843 Statistical Computing, Vienna, Austria.
- 844 **Raffaele S, Kamoun S. 2012.** Genome evolution in filamentous plant pathogens: why bigger can be
845 better. *Nature Reviews Microbiology* **10**: 417–430.
- 846 **Rice P, Longden L, Bleasby A. 2000.** EMBOSS: The European Molecular Biology Open Software
847 Suite. *Trends in Genetics* **16**: 276–277.
- 848 **Ritz C, Streibig JC. 2005.** Bioassay analysis using R. *Journal of Statistical Software* **12**: 1–22.
- 849 **Robinson JT, Thorvaldsdóttir H, Winckler W, Guttman M, Lander ES, Getz G, Mesirov JP.**
850 **2011.** Integrative Genome Viewer. *Nature Biotechnology* **29**: 24–6.
- 851 **Rogers PD, Barker KS. 2003.** Genome-wide expression profile analysis reveals coordinately
852 regulated genes associated with stepwise acquisition of azole resistance in *Candida albicans* clinical

- 853 isolates. *Antimicrobial Agents and Chemotherapy* **47**: 1220–1227.
- 854 **Rogers J, Gibbs RA. 2014.** Content and Dynamics. *Nature Reviews Genetics* **15**: 347–359.
- 855 **Rouxel T, Grandaubert J, Hane JK, Hoede C, van de Wouw AP, Couloux A, Dominguez V,**
856 **Anthouard V, Bally P, Bourras S, et al. 2011.** Effector diversification within compartments of the
857 *Leptosphaeria maculans* genome affected by Repeat-Induced Point mutations. *Nature*
858 *communications* **2**: 202.
- 859 **Sabeti PC, Varilly P, Fry B, Lohmueller J, Hostetter E, Cotsapas C, Xie X, Byrne EH,**
860 **McCarroll SA, Gaudet R, et al. 2007.** Genome-wide detection and characterization of positive
861 selection in human populations. *Nature* **449**: 913–918.
- 862 **SanMiguel P, Gaut BS, Tikhonov A, Nakajima Y, Bennetzen JL. 1998.** The paleontology of
863 intergene retrotransposons of maize. *Nature Genetics* **20**: 43–45.
- 864 **Shen RM, Batzer MA, Deininger PL. 1991.** Evolution of the master Alu gene(s). *Journal of*
865 *Molecular Evolution* **33**: 311–320.
- 866 **Simão FA, Waterhouse RM, Ioannidis P, Kriventseva E V., Zdobnov EM. 2015.** BUSCO:
867 Assessing genome assembly and annotation completeness with single-copy orthologs.
868 *Bioinformatics* **31**: 3210–3212.
- 869 **Singh NK, Chanclud E, Croll D. 2020.** Population-level deep sequencing reveals the interplay of
870 clonal and sexual reproduction in the fungal wheat pathogen *Zymoseptoria tritici*.
- 871 **Sirisattha S, Momose Y, Kitagawa E, Iwahashi H. 2004.** Toxicity of anionic detergents
872 determined by *Saccharomyces cerevisiae* microarray analysis. *Water Research* **38**: 61–70.
- 873 **Slotkin RK, Martienssen R. 2007.** Transposable elements and the epigenetic regulation of the
874 genome. *Nature Reviews Genetics* **8**: 272–285.
- 875 **Soustre I, Letourneux Y, Karst F. 1996.** Characterization of the *Saccharomyces cerevisiae* RTA1
876 gene involved in 7-aminocholesterol resistance. *Current Genetics* **30**: 121–125.
- 877 **Stöver BC, Müller KF. 2010.** TreeGraph 2: Combining and visualizing evidence from different
878 phylogenetic analyses. *BMC Bioinformatics* **11**: 1–9.
- 879 **Stritt C, Gordon SP, Wicker T, Vogel JP, Roulin AC. 2017.** Recent activity in expanding
880 populations and purifying selection have shaped transposable element landscapes across natural
881 accessions of the Mediterranean grass *Brachypodium distachyon*. *Genome Biology and Evolution*
882 **10**: 1–38.
- 883 **Stuart T, Eichten SR, Cahn J, Karpievitch Y V, Borevitz JO, Lister R. 2016.** Population scale
884 mapping of transposable element diversity reveals links to gene regulation and epigenomic variation.
885 *eLife* **5**: 1–27.
- 886 **Stukenbrock EH, Banke S, Javan-Nikkhah M, McDonald BA. 2007.** Origin and domestication of
887 the fungal wheat pathogen *Mycosphaerella graminicola* via sympatric speciation. *Molecular Biology*
888 *and Evolution* **24**: 398–411.
- 889 **Stukenbrock EH, Bataillon T, Dutheil JY, Hansen TT, Li RQ, Zala M, McDonald BA, Wang J,**
890 **Schierup MH. 2011.** The making of a new pathogen: Insights from comparative population
891 genomics of the domesticated wheat pathogen *Mycosphaerella graminicola* and its wild sister
892 species. *Genome Research* **21**: 2157–2166.
- 893 **Torriani SFF, Melichar JPE, Mills C, Pain N, Sierotzki H, Courbot M. 2015.** *Zymoseptoria*
894 *tritici*: A major threat to wheat production, integrated approaches to control. *Fungal Genetics and*
895 *Biology* **79**: 8–12.
- 896 **Walser J-C, Chen B, Feder ME. 2006.** Heat-Shock Promoters: Targets for Evolution by P
897 Transposable Elements in *Drosophila*. *PLOS Genetics* **2**: e165.
- 898 **Waterhouse AM, Procter JB, Martin DMA, Clamp M, Barton GJ. 2009.** Jalview Version 2-A
899 multiple sequence alignment editor and analysis workbench. *Bioinformatics* **25**: 1189–1191.
- 900 **Wickham H. 2016.** *ggplot2: Elegant Graphics for Data Analysis*. New York: Springer-Verlag.
- 901 **Wickham H, Chang W. 2016.** devtools: Tools to Make Developing R Packages Easier.
- 902 **Wong WY, Simakov O, Bridge DM, Cartwright P, Bellantuono AJ, Kuhn A, Holstein TW,**

- 903 **David CN, Steele RE, Martínez DE. 2019.** Expansion of a single transposable element family is
904 associated with genome-size increase and radiation in the genus *Hydra*. *Proceedings of the National*
905 *Academy of Sciences* **116**: 22915–22917.
- 906 **Yew SM, Chan CL, Kuan CS, Toh YF, Ngeow YF, Na SL, Lee KW, Hoh CC, Yee WY, Ng KP.**
907 **2016.** The genome of newly classified *Ochroconis mirabilis*: Insights into fungal adaptation to
908 different living conditions. *BMC Genomics* **17**: 1–17.
- 909 **Zhan J, Kema GHJ, Waalwijk C, McDonald BA. 2002.** Distribution of mating type alleles in the
910 wheat pathogen *Mycosphaerella graminicola* over spatial scales from lesions to continents. *Fungal*
911 *Genetics and Biology* **36**: 128–136.
- 912 **Zhan J, Linde CC, Jurgens T, Merz U, Steinebrunner F, McDonald BA. 2005.** Variation for
913 neutral markers is correlated with variation for quantitative traits in the plant pathogenic fungus
914 *Mycosphaerella graminicola*. *Mol Ecol* **14**: 2683–2693.
- 915 **Zhan J, Pettway RE, McDonald BA. 2003.** The global genetic structure of the wheat pathogen
916 *Mycosphaerella graminicola* is characterized by high nuclear diversity, low mitochondrial diversity,
917 regular recombination, and gene flow. *Fungal Genetics and Biology* **38**: 286–297.
- 918 **Zheng X, Gogarten SM, Lawrence M, Stilp A, Conomos MP, Weir BS, Laurie C, Levine D.**
919 **2017.** SeqArray-a storage-efficient high-performance data format for WGS variant calls.
920 *Bioinformatics* **33**: 2251–2257.
- 921 **Zheng X, Levine D, Shen J, Gogarten SM, Laurie C, Weir BS. 2012.** A high-performance
922 computing toolset for relatedness and principal component analysis of SNP data. *Bioinformatics* **28**:
923 3326–3328.
- 924
- 925

926 **Figure Legends**

927

928 **Figure 1: Robust discovery and validation of transposable element (TE) insertions:** (A) General
929 analysis pipeline. (B) Read depth down-sampling analysis for one isolate per population with an
930 average coverage of the population. The vertical black line indicates the coverage at which on average
931 90% of the maximally detectable variants were recovered. Dashed black lines indicate the standard
932 error. The threshold for a minimal mean coverage was set at 15X (red line). (C) Validation of
933 insertions absent in the reference genome. (i) TE insertions that are not present in the reference
934 genome show a duplication of the target site and the part of the reads that covers the TE will not be
935 mapped against the reference genome. We thus expect reads to map to the TE surrounding region and
936 the target site duplication but not the TE itself. At the target site, a local duplication of read depth is
937 expected. (ii) We selected all reads in an interval of 100 bp up- and downstream including the target
938 site duplication to detect deviations in the number of reads terminating near the target site duplication.
939 (D) Validation of insertions present in the reference genome. (i) Analyses read coverage at target site
940 duplications. (ii) Decision map if a TE should be kept as a true insertion or rejected as a false positive.
941 Only predicted TE insertions that overlap evidence of split reads were kept as TE insertions in
942 downstream analyses. (E) Singleton validation using long-read PacBio sequencing. (i) Analysis if TE
943 insertions overlap with a detected insertion/deletion locus (Badet *et al*, 2021). (ii) Homology search of
944 the TE insertion flanking sequences based on the reference genome against PacBio reads. In addition,
945 the consensus sequence of the inserted TE was used for matches between the flanks.

946 **Figure supplement 1.** Validation of transposable element (TE) insertion predictions. (A) TEs not
947 present in the reference genome: distribution of additional TE hits found per locus after the outlier
948 test. Color indicates superfamilies. (B) TEs not present in the reference genome: distribution of
949 additional TE hits found per population after the outlier test. Colors indicate populations. (C) TEs
950 present in the reference genome: distribution of missing data per locus after the validation with
951 spliced junction reads. Missing data indicates that the TE was not predicted with `ngs_te_mapper` and
952 that there was no indication of spliced reads. The red line (=20 %) indicates the threshold for missing
953 data. TE loci with an amount of missing data > 20 % were completely excluded from further analyses.
954 Color indicates superfamily. (D) TEs present in the reference genome: detection of strong outlier
955 isolates with a high number of split reads. Color indicates the population.

956 **Figure supplement 2.** TE insertion validations for non-reference copies (Table).

957 **Figure supplement 3.** Establishment of transposable element (TE) loci with differing start and end
958 positions in the isolates. Distribution of length of distance for start position, end position and both
959 start and end combined after the correction.

960 **Figure supplement 4.** Bias for reads with a GC content lower than 30 % per population. Red lines
961 indicate the mean.

962 **Figure supplement 5.** TE consensus sequences (Table).

963

964 **Figure 2: Transposable element (TE) landscape across populations.** (A) Allele frequencies of the
965 TE insertions across all isolates. (B) TE insertions per Mb on core chromosomes (dark) and accessory
966 chromosomes (light). Dashed lines represent mean values. Blue: global mean of 75.65 insertions/Mb,
967 dark: core chromosome mean of 58 TEs/Mb, light: accessory chromosome mean of 102.24
968 insertions/Mb). (C) Number of TE insertions per family. (D) TE frequencies among isolates and copy
969 numbers across the genome. The blue line indicates the maximum number of isolates ($n = 284$). (E)
970 Allele frequency distribution of TE insertions into introns and exons. (F) Number of TE insertions
971 within 1 kb up- and downstream of genes on core chromosomes including introns and exons (100 bp
972 windows). The blue arrow indicates a gene schematic with exons and an intron, the green triangles
973 indicate TE insertions. The dotted blue line indicates no deviation from the expected value (*i.e.*, mean
974 number of TEs per window).

975 **Figure supplement 1.** TEs in reference (Table).

976 **Figure supplement 2.** Validation of singleton insertions detected by mapped Illumina reads using
977 PacBio read alignments for confirmation. (A) Comparison of TE family copy numbers per isolate to
978 the number of copies found in the reference genome (IPO323). The color is indicating superfamilies.
979 This figure includes only TE families that were detected in any of the isolates used for validation. (B)
980 Confirmation of singleton TE insertions detected in the isolates CH99_SW5, CH99_SW39,
981 CH99_3D7, CH99_3D1, ISR92_Ar_4f, AUS01_1H8 and ORE90Ste_4A10 using aligned PacBio
982 reads. Confirmed/not confirmed TE insertions are shown by TE family. (C) PacBio read coverage (in
983 500 bp window) at singleton loci.

984 **Figure supplement 3.** Presence absence matrix TE loci (Table).

985 **Figure supplement 4.** Singletons (Table).

986 **Figure supplement 5.** TE insertion loci characteristics. (A) Number of TE insertions and density
987 (insertions per Mb) in accessory and core genes. (B) Allele frequencies of TEs genome-wide and
988 restricted to recombination hotspots. (C) TE insertion density and TE copy numbers within and
989 outside of recombination hotspots.

990 **Figure supplement 6.** Hierarchy superfamilies. (A) Number of transposable element (TE) insertions
991 per superfamily. Colors indicate the superfamily. (B) Number of TE loci and classification hierarchy.
992 (C) Comparison of mean genome sequencing coverage and the number of detected TEs with
993 ngs_te_mapper in isolates of the Middle East population. Dots indicate the coverage and colors
994 indicate the superfamily.

995

996 **Figure 3: Differentiation in transposable element insertions frequencies across the genome.** (A)
997 Global pairwise F_{ST} distributions shown across the 21 chromosomes. The red horizontal line indicates
998 the mean F_{ST} ($= 0.0163$). TEs with a strong local short-term frequency difference among populations
999 are highlighted (blue: increase in Europe; green: increase in North America). (B) Allele frequency

1000 changes between the populations. The same TE loci as in panel A are highlighted. (C) Circos plot
1001 describing from the outside to the inside: The black line indicates chromosomal position in Mb. Blue
1002 bars indicate the gene density in windows of 100 kb with darker blue representing higher gene
1003 density. Red bars indicate the TE density in windows of 100 kb with a darker red representing higher
1004 TE density. Green triangles indicate positions of TE insertions with among population F_{ST} value
1005 shown on the y-axis.

1006 **Figure supplement 1.** Global pairwise F_{ST} distributions shown separately for the 21 chromosomes.
1007 The red horizontal line indicates the mean $F_{ST} = 0.0163$. Colors are according to the three main
1008 superfamilies (RLG, RLC, DHH).

1009

1010 **Figure 4: Candidate adaptive transposable element (TE) insertions.** (A) Distribution of all
1011 extremely differentiated TEs and their distance to the closest gene. Color indicates the superfamily.
1012 The stars indicate TE insertions not found in the reference genome. (B) Location of the RLG_Luna
1013 TE insertion on chromosome 12 corresponding to its two closest genes. (C) Resistance against azole
1014 fungicides among isolates as a function of TE presence or absence. (D) Genomic niche of the
1015 RLG_Luna TE insertion on chromosome 12: F_{ST} values for each TE insertion, gene content (blue), TE
1016 content (green) and GC content (yellow). The grey section highlights the insertion site. (E) Number of
1017 RLG_Luna copies per isolate and population. (F) Frequency changes of RLG_Luna between the two
1018 North American populations compared to the other populations. Colors indicate the number of copies
1019 per chromosome. (G) Phylogenetic trees of the coding sequences of either the gene encoding the
1020 RTA1-like protein or the protein kinase domain. Isolates of the two North American populations and
1021 an additional 11 isolates from other populations not carrying the insertion are shown. Blue color
1022 indicates TE presence, yellow indicates TE absence.

1023 **Figure supplement 1.** Top loci information (Table).

1024 **Figure supplement 2.** Additional top loci. Six additional candidate adaptive transposable element
1025 (TE) insertions. Each row corresponds to a candidate, with the first five being candidates detected in
1026 the North American populations and the last one in the European populations. For each candidate, the
1027 direction of the TE and the direction, function and distance of the closest two genes are indicated. The
1028 middle column indicates the location of the TE in the genomic niche, with TE content, gene content
1029 and GC content for the surrounding windows. The third column indicates resistance levels towards
1030 azole antifungals for isolates with and without the TE insertion.

1031

1032 **Figure 5: Population differentiation at transposable element (TE) and genome-wide SNP loci.**
1033 (A) Sampling locations of the six populations. Middle East represents the region of origin of the
1034 pathogen. In North America, the two populations were collected at an interval of 25 years in the same
1035 field in Oregon. In Europe, two populations were collected at an interval of 17 years from two fields
1036 in Switzerland <20 km apart. Dark arrows indicate the historic colonization routes of the pathogen.

1037 (B) Principal component analysis (PCA) of 284 *Zymoseptoria tritici* isolates, based on 900,193
1038 genome-wide SNPs. (C) PCA of a reduced SNP data set with randomly selected 203 SNPs matching
1039 approximately the number of analyzed TE loci. (D) PCA based on 193 TE insertion loci. Loci with
1040 allele frequency < 5% are excluded.

1041 **Figure supplement 1.** Isolates (Table).

1042

1043 **Figure 6: Global population structure of transposable element (TE) insertion polymorphism.**

1044 (A) Total TE copies per isolate. Colors identify TE superfamilies. (B) TE copies per family and (C)
1045 superfamily. (D) TE insertion frequency spectrum per population. The curve fitting was performed
1046 with a self-starting NIs asymptomatic regression model (E). TE family copy numbers per isolate.

1047 **Figure supplement 1.** Population changes additional. Variation in transposable element (TE) content
1048 per isolate across populations. (A) Total TE copies per superfamily (colored) and per isolate only
1049 including LTR (long terminal repeat) TEs *Copia* and *Gypsy*. Color indicates the family. (B) Total TE
1050 copies per superfamily (colored) and per isolate only on the core chromosomes. (C) Total TE copies
1051 per superfamily (colored) and per isolate only on the accessory chromosomes.

1052 **Figure supplement 2.** Kolmogorof-Smirnov (Table).

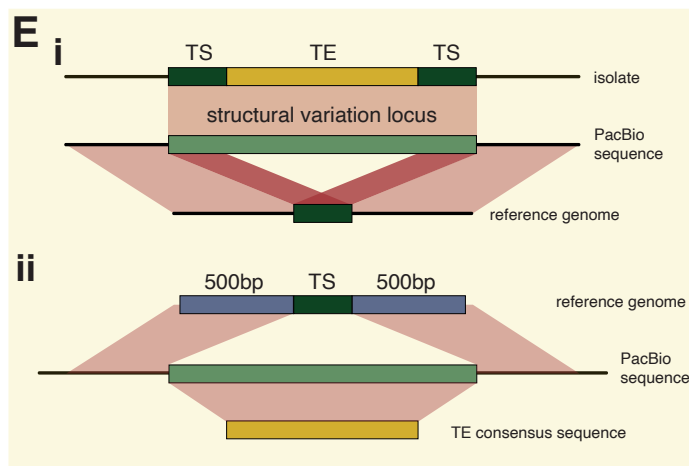
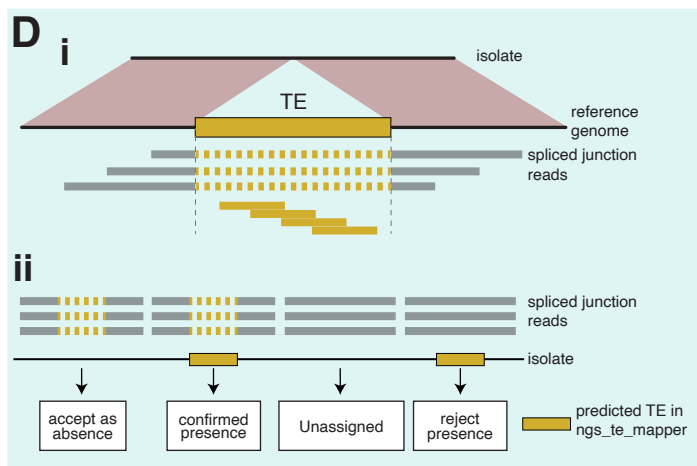
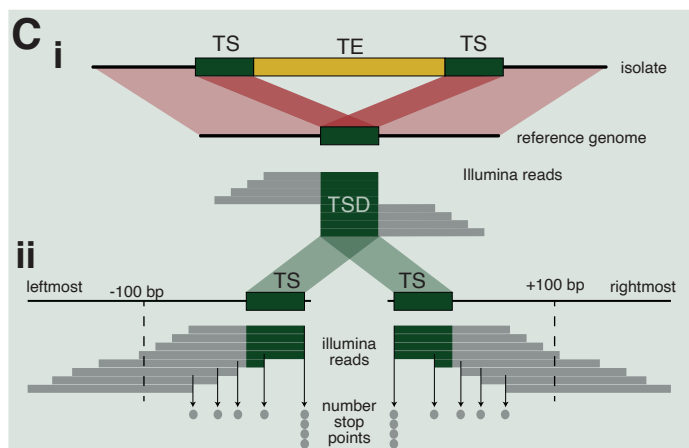
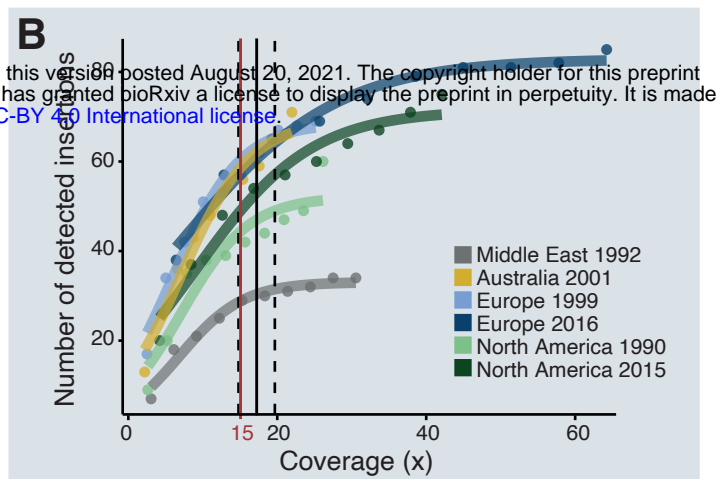
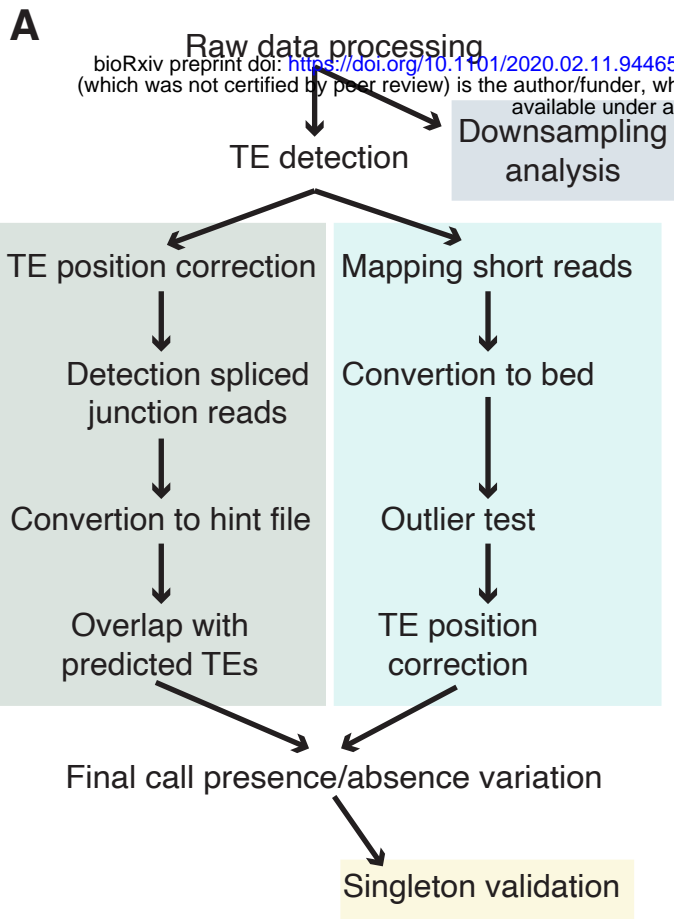
1053 **Figure supplement 3.** Heatmap loci. (A) Presence (blue) and absence (yellow) matrix for all
1054 transposable element (TE) loci in all isolates per population. Colors on the left side indicate the
1055 superfamily. (B) Comparison of different genomic regions with and without TE insertions in IPO323.

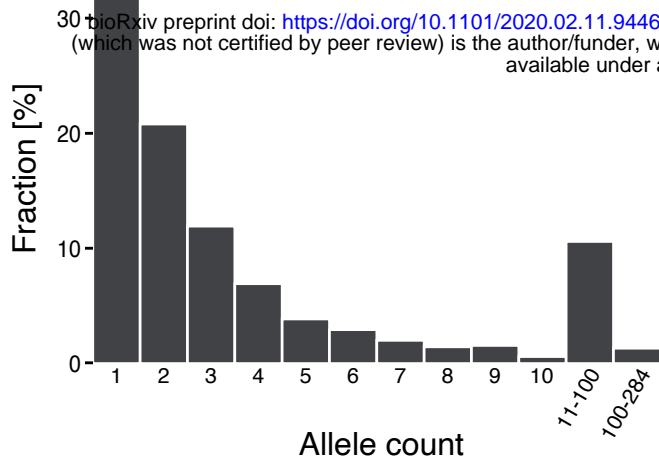
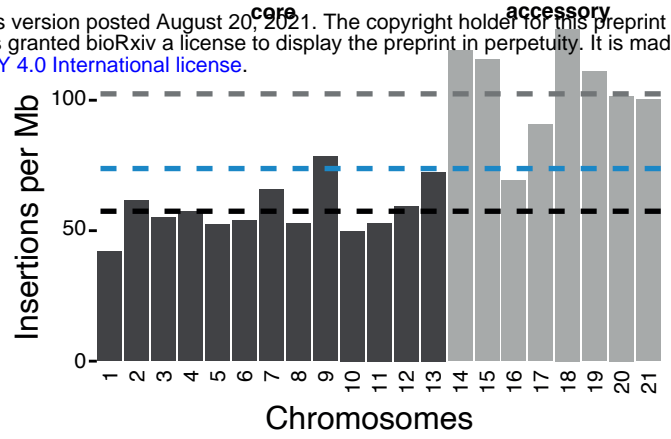
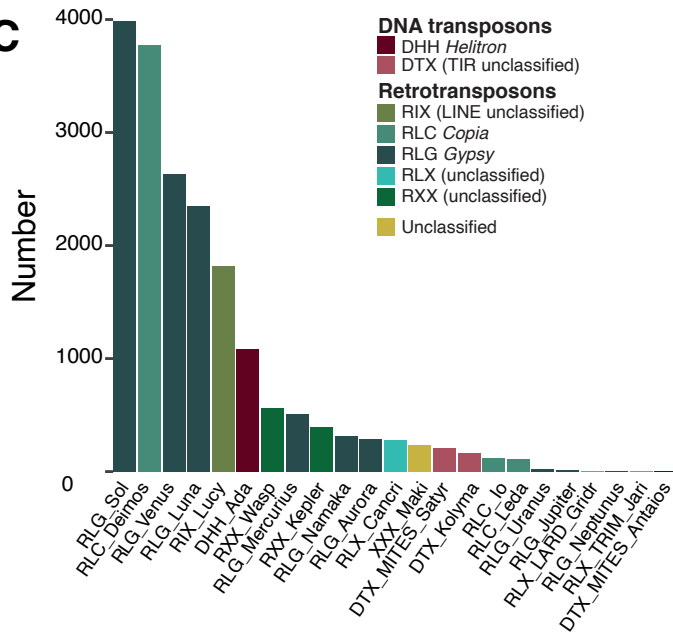
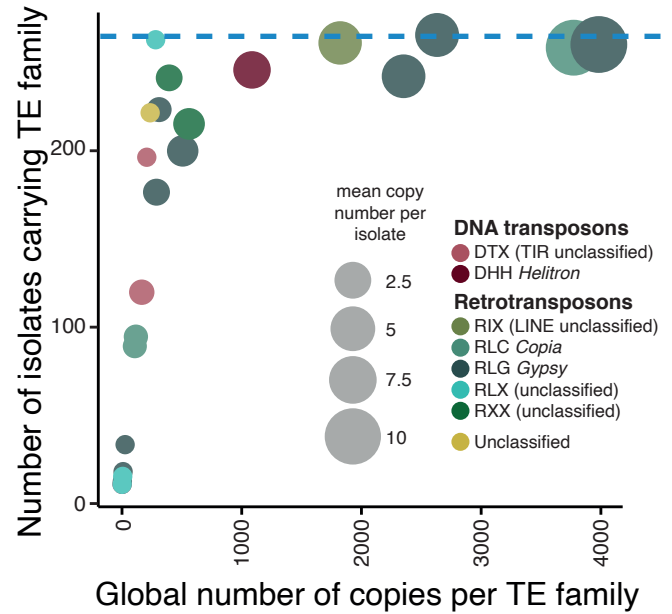
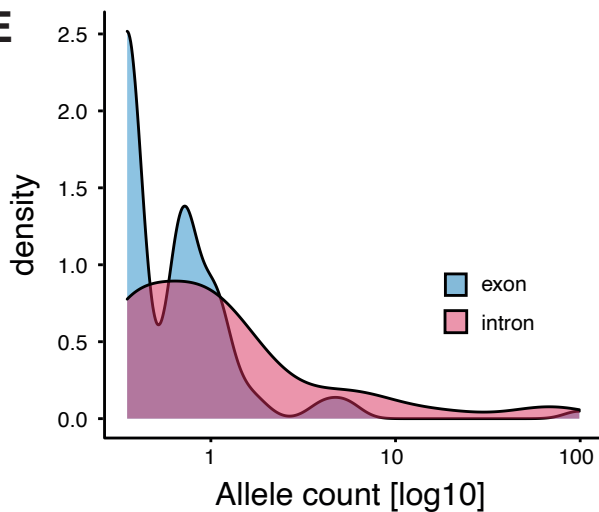
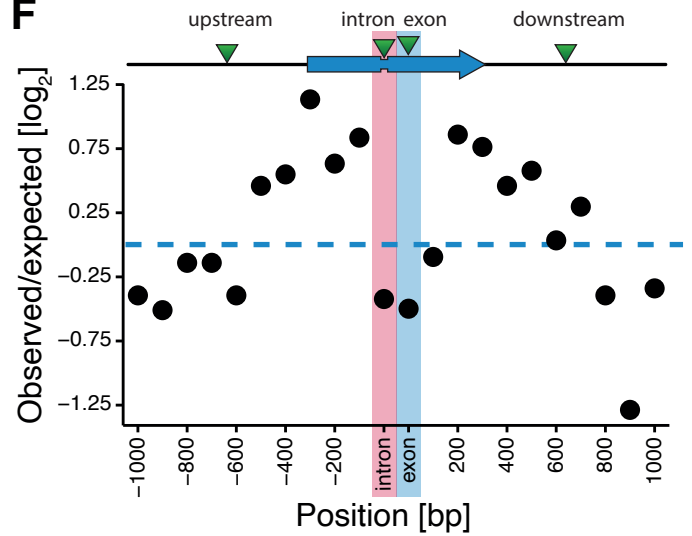
1056

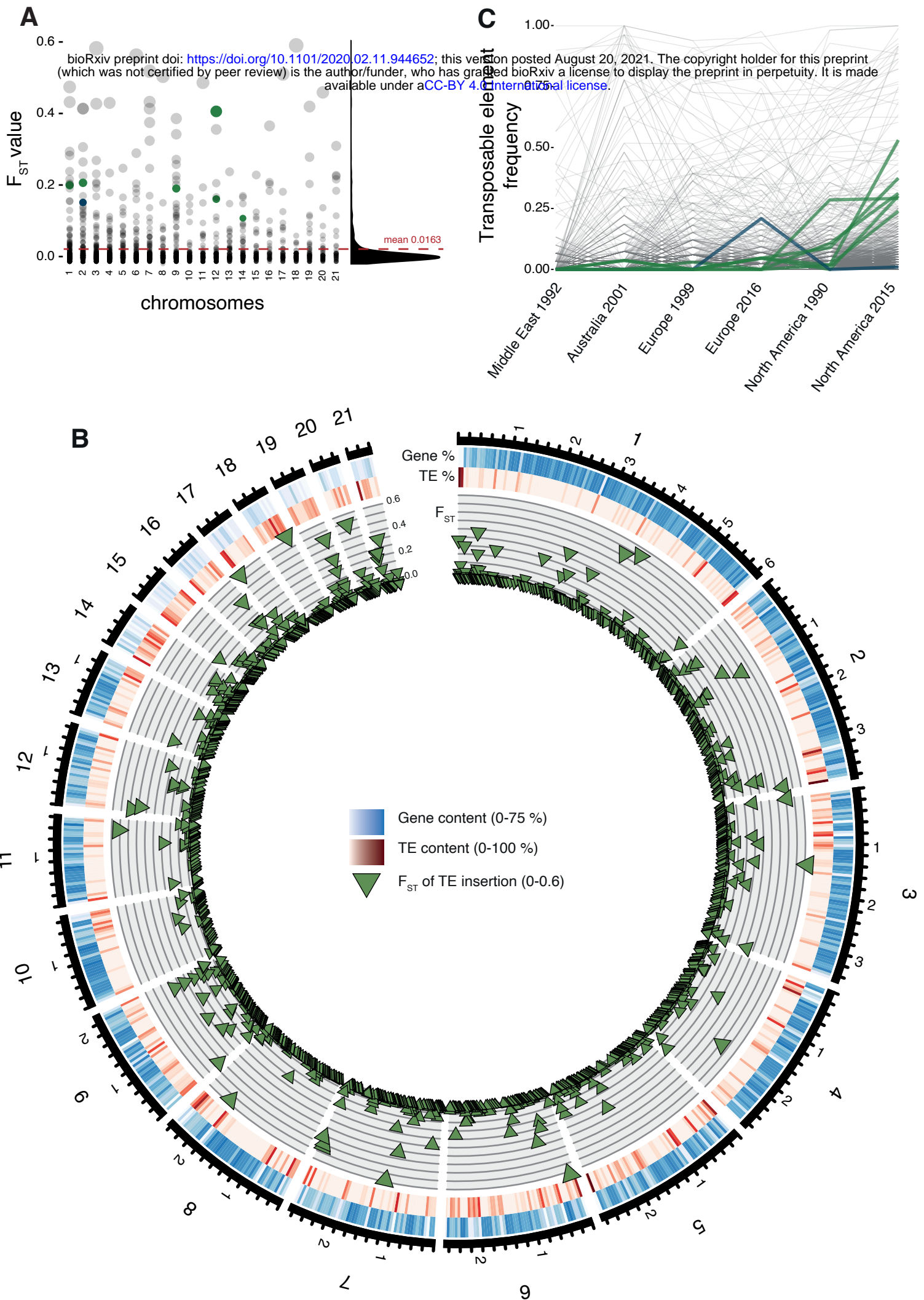
1057 **Figure 7: Core genome size and transposable element (TE) evolution across populations.** (A)

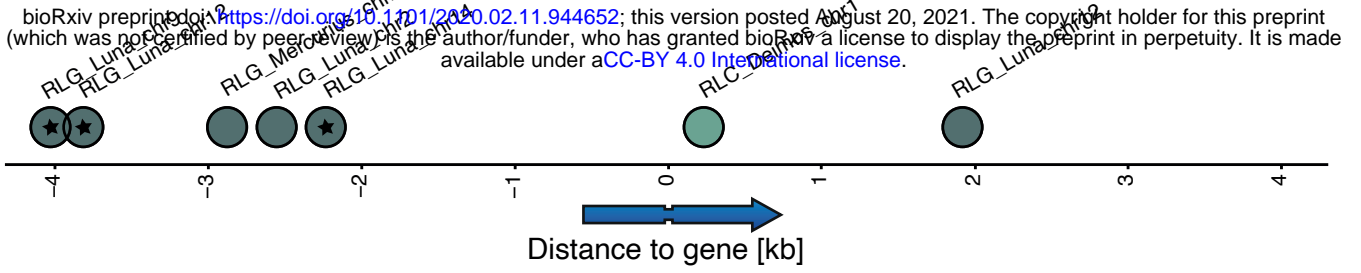
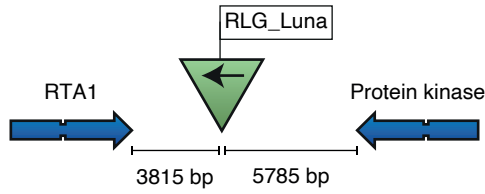
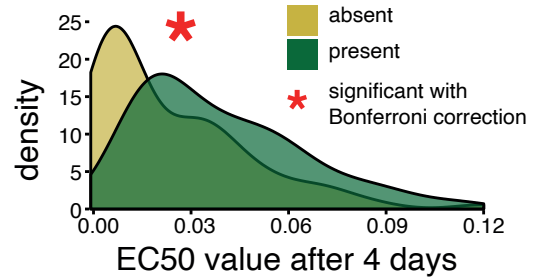
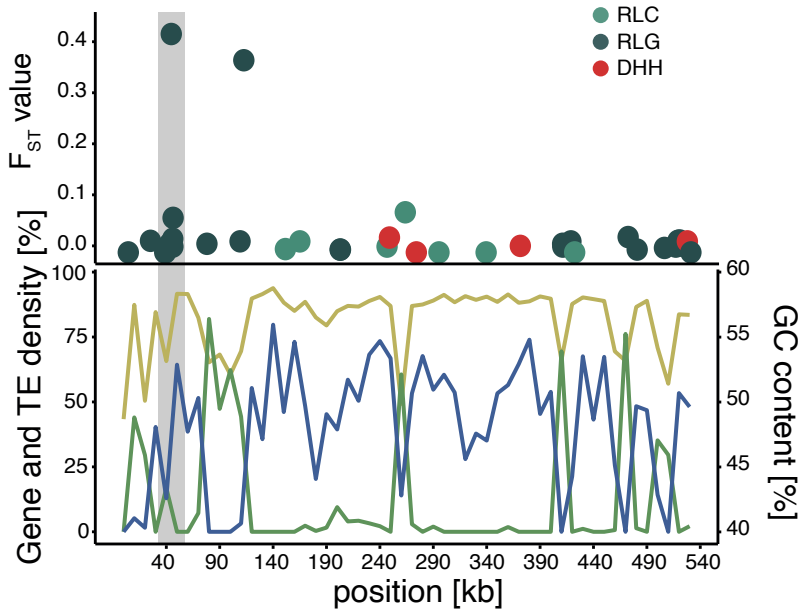
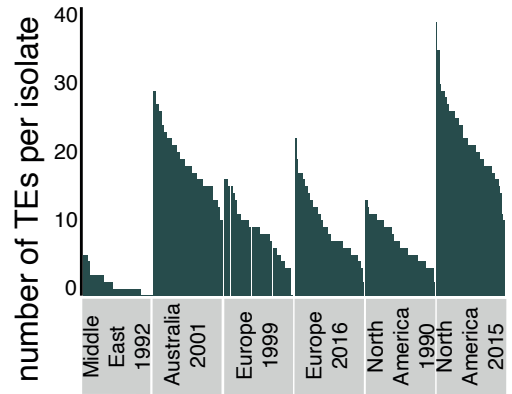
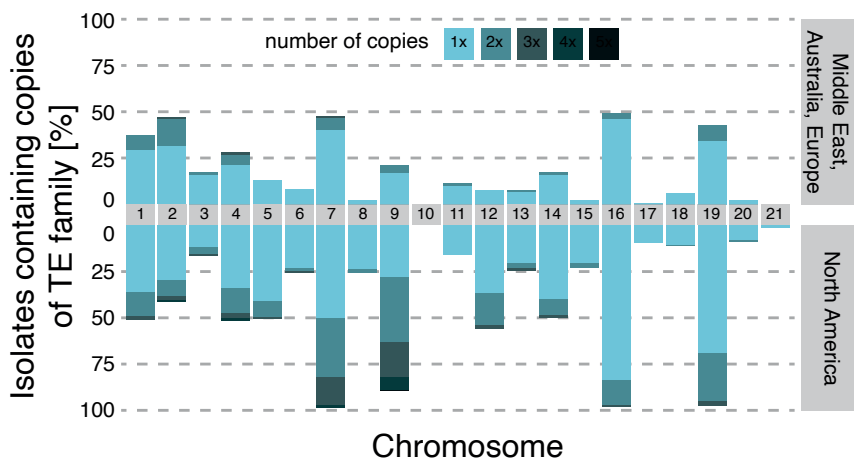
1058 BUSCO completeness variation among genome assemblies. Black lines indicate the mean genome
1059 size per population. (B) Genome-wide GC content variation. (C) Core genome size variation among
1060 the isolates of the populations (excluding accessory chromosomes). (D) Correlation of core genome
1061 size and number of detected TEs. (E) Correlation of core genome size and the cumulative length of all
1062 TEs detected as inserted. (F) Correlation of core genome size and genome-wide GC content. (G)
1063 Spearman correlation matrix of BUSCO completeness, core genome size, number of detected TEs and
1064 genome-wide GC content.

1065 **Figure supplement 1.** Genome size expansion. (A) Estimated length of TE insertions per isolate and
1066 population. (B) Genome size variation per population. (C) Percentage of TEs content variation
1067 compared to the variation in genome size. (D) TE contributions to genome size variation compared to
1068 full genome size.

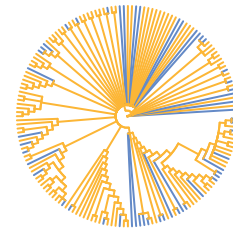


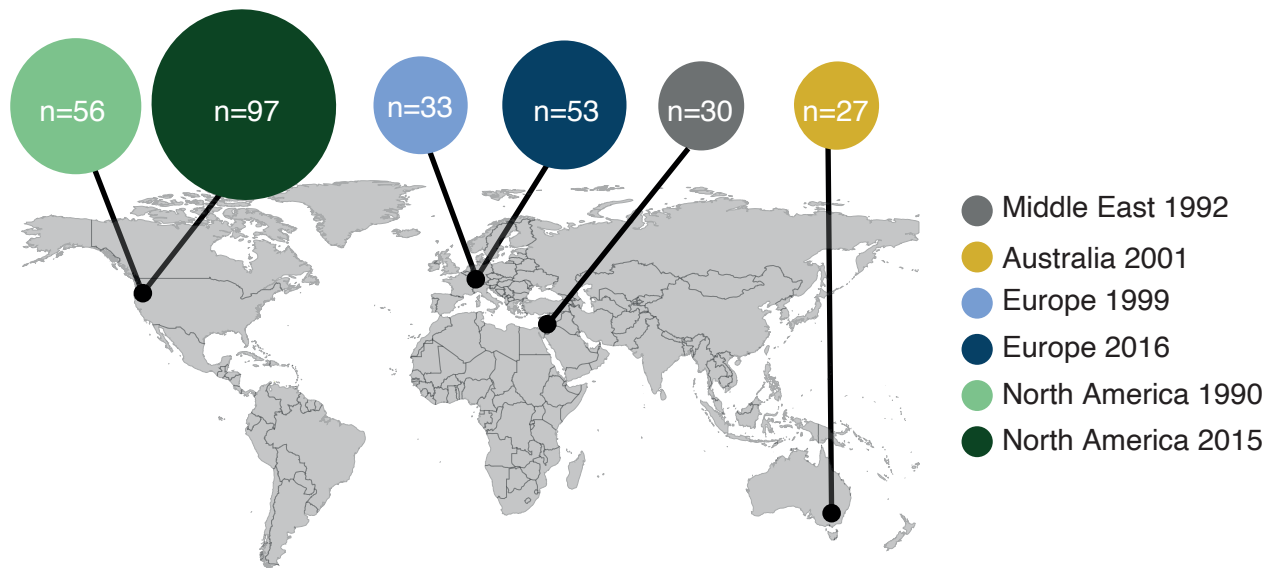
A**B****C****D****E****F**



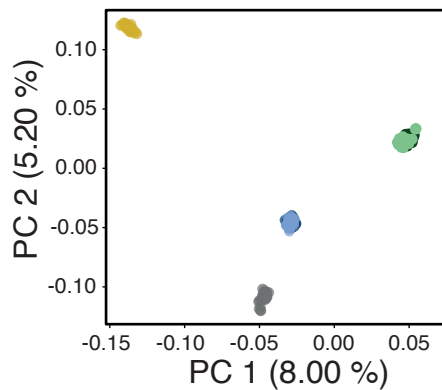
A**B****C****D****E****F****G** RTA1 like protein

Protein kinase domain

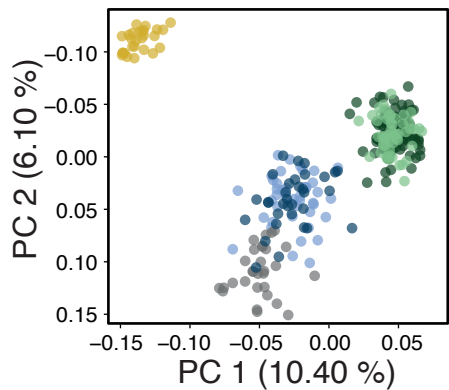


A**B**

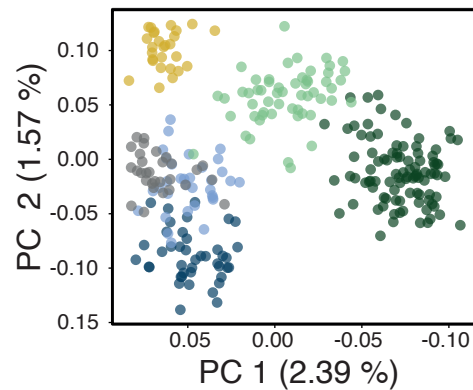
Genome-wide SNPs

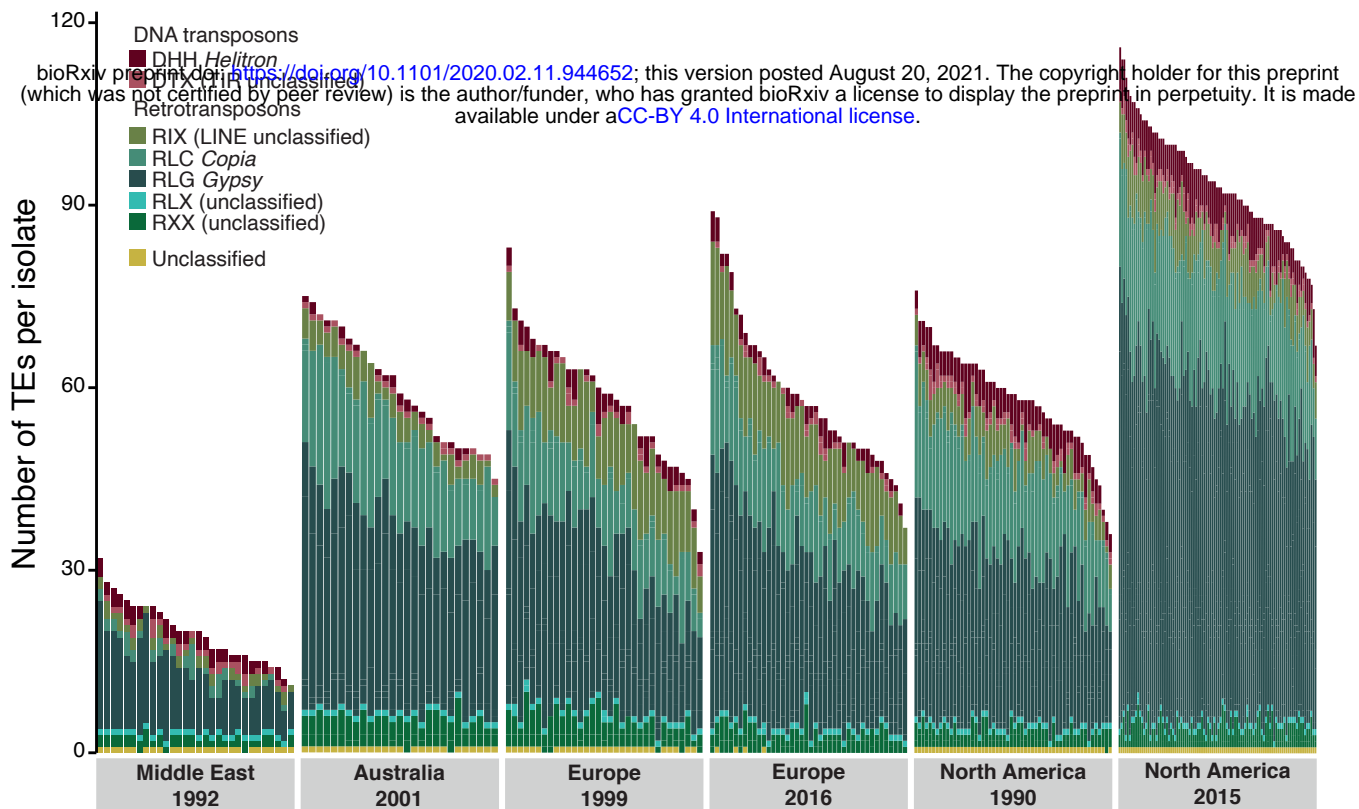
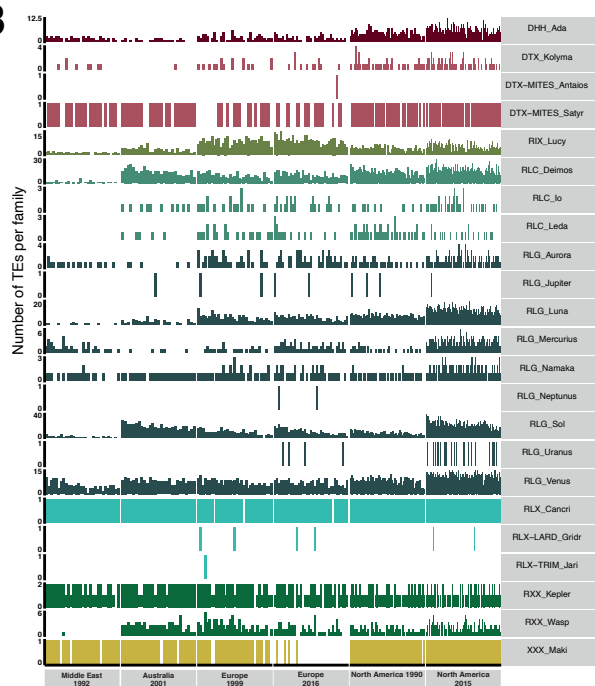
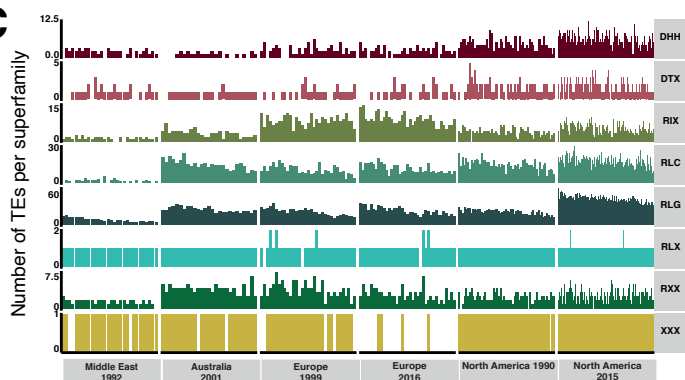
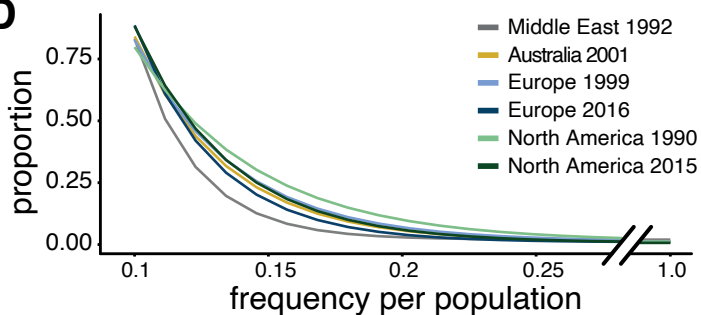
**C**

Genome-wide SNPs (subset)

**D**

Transposable element loci



A**B****C****D****E**